

A Customized Novel Halo with Displacement Based Pin Tightening for Pre-Operative Gravity Traction to Treat Severe Scoliosis

Written by
Wolf Botterman 2018



UMC Utrecht





DELFT UNIVERSITY OF TECHNOLOGY
Department of Biomedical Engineering

MASTER THESIS

A Customized Novel Halo with Displacement Based Pin Tightening for Pre-Operative Gravity Traction to Treat Severe Scoliosis

by
WOLF BOTTERMAN

to be defended on September 27, 2018 at 10:00

Project duration: November 15, 2017 - September 27, 2018

Student number: 4101685

Committee: Dr. Jie Zhou
Ir. Jesse Bosma
Dr. Vera Popovich
Dr. ir. Joost de Winter

TU Delft, supervisor
MTKF (UMC Utrecht), supervisor
TU Delft
TU Delft

Preface

Dear reader, you are about read a thesis which closes my final chapter of 8 pleasant years of studying at the Technical University of Delft. The past 10 months of graduating have been exciting for me. I enjoyed the close collaboration with clinicians at UMC Utrecht and the freedom of exploring and solving problems which came about during the project. I learned a lot about patients with severe scoliosis who are being treated by Halo Gravity Traction and made me realize the importance of this kind of research.

I want to thank everybody who helped me put together these 10 months, because without this help I would not have been able to get this result.

Donations to science People donating their body are of great scientific value. Even though I have not known the person who donated his body to science, I would like to thank him in doing so. Because of this person, quick iterations could be made and eventually a big step was taken in the fabrication and evaluation of a new halo.

Jie Thank you for our qualitative technical discussions and the provided research directions you proposed in order to guide me. I really appreciate the time you were willing to spent to help me improve my thesis. Your positive attitude and our funny conversations made me enjoy our collaboration very much. I wish you all the best and hope to see you again.

Jesse Your practical solutions to some of my problems helped me a lot in continuing my research. I enjoyed our collaboration and your quick help when I asked for it. I also want to thank all others of the department of MTKF for their pleasant way of working. I have always felt comfortable at MTKF which contributed to the enthusiasm of executing this research. Also the off-topic conversations contributed to a relaxed working atmosphere.

Moyo en Mendel Next to the project, I have learned a lot thanks to you guys. Due to your openness, I have experienced a lot more aspects of the UMC Utrecht than I initially had thought, prior to this project. Thanks in part to your enthusiasm and practical approach, a very nice step has been made in the field of Halo Gravity Traction and I am looking forward to see the halo in clinical practice.

Kevin Thank you for the nice and open collaboration. I enjoyed seeing our work merge together in the new halo ring and I wish you all the luck at your new job.

Jos Thank you for helping me with the application of the strain gauges. Also I enjoyed your conversations and your clarifying explanations on difficult topics.

Jolijn Due to your support and willingness to listen and understand some of my bottlenecks during the project, I was able to relieve stress by talking about it. It was nice to see how quickly you understood some of the harder technical subjects in this project and discuss with me about it.

Family I want to thank my family and mother in law for helping me during this thesis. I appreciate the interest you guys had in my work, which helped me zoom out of the project and look at it from different perspectives. The coffee breaks, with specially brewed coffee, made me clear my mind. As a closing word of thanks, I would like to thank my parents in special for their 8-year during support, as well physically as financially. Without you, I would never could have get where I am right now.

Abstract

Severe scoliosis is a deformity of the curvature of the spine, mostly occurring in children. It is currently treated by performing Halo Gravity Traction (HGT) to reduce the curvature prior to surgery. In this procedure, a Bremer halo ring is fitted around the child's head and connected to the skull with a number of pins. During the 3-month treatment period, step-wise increased weight is applied to pull the ring upwards so as to elongate the spine. With the current design of the Bremer halo ring, the pins are tightened while measuring the amount of torque applied, influences each other during tightening, loosen over time and leave visible scars on the forehead. Furthermore, the Bremer halo ring is not customized.

In the present project, a novel halo with a different tightening technique was designed, manufactured and evaluated with the aim of solving the above mentioned shortcomings of the Bremer halo.

A Surface Tessellation Language (STL) file was generated from Computed Tomography (CT) images of a male cadaver head. Based on the desired ring stiffness and the geometry of a custom-designed halo for the cadaver head, a model was created in Solid Edge ST 10. The model was analyzed and adjusted by using the Finite Element Method (FEM). The customized halo ring was then produced by means of Selective Laser Sintering (SLS) and then equipped with strain gauges in order to derive the forces acting on the skull by the pins during tightening. The customized novel halo and the Bremer halo were compared with respect to moment arm and pin orientation, both influencing the local pin site behavior. The moment arms, pin positions and pin orientations of the 3D model of the novel halo were validated in reality by consecutive application of the halo to the cadaver head. The halo was analyzed by measuring the pin force degradation over a period of 24 h, which was hypothesized to be caused by the visco-elastic behavior of the skull of the cadaver head. The tightening procedure was analyzed on a block of steel to determine the influence on the axial pin reaction forces.

The novel halo showed smaller and more consistent lengths of moment arm than the Bremer halo. Furthermore, one pin of the Bremer halo showed a difference of $>15^\circ$ from 90° , which has been regarded as contributor to pin loosening. The novel halo was predicted to be able to keep sufficient axial pin force without pin re-tightening during the traction period. The intended axial pin forces of the novel halo were achieved with an accuracy of 94.5%.

With the customized novel halo, pins were tightened based on the displacement of the C-contours, resulting in an increased accuracy of pin force during tightening. The anterior pins were designed to be located in the musculus temporalis region, thereby leaving no visible scars and to be less prone to loosening due to a lower anterior ring stiffness. In conclusion, customizing the halo ring brings opportunities to engineer and control important parameters which contribute to better wearing comfort, higher pin force accuracy and less pin loosening, although it is yet a costly and time-consuming procedure.

Contents

1	Introduction	8
1.1	Background	8
1.2	HGT at UMC Utrecht	10
1.3	Problem identification	11
1.3.1	Improper fit around the cranium	11
1.3.2	Pin loosening	11
2	Shortcomings of the Bremer halo	12
2.1	Improper fit around the cranium	13
2.1.1	Generalized ring	13
2.1.2	Visible scars	13
2.2	Pin loosening	14
2.2.1	Spring characteristics	14
2.2.2	Undefined pin reaction forces	15
2.2.3	Torque-based tightening	17
3	Novel halo	19
3.1	General objective	19
3.2	Design process	20
3.3	Anterior pin location	22
3.4	Posterior pin location	22
3.5	Pins	23
3.6	The novel halo	23
4	Research	25
5	Part I Customization	27
5.1	Methods	28
5.2	Results	30
5.2.1	Experiment 1	30
5.2.2	Experiment 2	31
5.3	Discussion	34
5.4	Conclusions	35
5.4.1	Experiment 1	35
5.4.2	Experiment 2	35
5.4.3	General	35
6	Part II. Axial pin force control	36
6.1	Visco-elasticity of the cadaver head	37
6.1.1	Methods	37
6.1.2	Results	40
6.1.3	Discussion	42
6.1.4	Conclusion	42
6.2	Pin reaction forces	43
6.2.1	Methods	43
6.2.2	Results	44
6.2.3	Discussion	46
6.2.4	Conclusion	47
7	General discussion	48
8	General conclusion	49
9	Recommendations	51
10	References	53
11	Appendix	55



A Analysis of the Stiffness of the Bremer Halo	55
A.1 Displacement at posterior pin sites - Experimental measurement	55
A.2 Displacement at posterior pin sites - FEM	56
A.3 Displacement at anterior pin sites - FEM	58
B Requirements	59
C Design concepts	60
D Novel Halo - Parameter Determination	62
D.1 Geometry determination	62
D.2 Displacements at anterior and posterior pin sites - FEM	64
D.3 Displacement at anterior and posterior pin sites - experimental measurements	65
E Relationship between Torque and Force in the Bremer halo	67
F Strain Gauges	68
F.1 Anterior ring of novel halo	68
F.2 Posterior ring of the novel halo	69
F.3 Calibration of strain gauges	70
F.4 Technical data of strain gauges	71
G Traction Force	72

1 Introduction

1.1 Background

There are several types of spinal curvature deformities described by the deviations from the anatomical planes, as illustrated in Figure 1. Scoliosis is a deformity of the spine, predominantly described as an 'S-shaped' curve of the spine in the coronal plane as shown in Figure 2a. Kyphoscoliosis is a twist of the curve in the sagittal and coronal planes. Healthy spines do not have a curvature in any of these planes.

Treating severe scoliosis and kyphoscoliosis remains a surgical challenge. Reducing spinal curvatures and straightening the spine may not be achieved by one single operation, if the spinal curvature is too great. In clinical practice, pre-surgical halo gravity traction (HGT) is often applied first to reduce the curvature as shown in Figure 2b. After a considerable reduction in spinal curvature a surgical procedure called spondylosis is effectively performed. Spondylosis is achieved via the guidance of the spinal curve along two stainless steel rods located lateral to the processus spinosus which are inserted along the spine. Figure 2c shows the result of spondylosis.

The severity of scoliosis and kyphoscoliosis is indicated by the Cobb angle, which is a quantitative indicator for the severity of the curvature of the spine in the coronal plane. An angle of $\geq 100^\circ$ indicates severe scoliosis[2]. When the Cobb angle exceeds 80° , 85% of surgeons perform pre-operative traction on the scoliotic spine[3]. Traction is perpendicular to the transverse plane, as illustrated in Figure 1. The vector is generated by a weight, which acts continuously in the gravitational direction. This weight is applied to a halo, which is connected to the patient's skull with pins. The skull then pulls via the first vertebra C1 on the remaining spine, where the mass of the body acts as a counterweight. This procedure, as schematically illustrated in Figure 3, is called 'halo gravity traction'.

While some patients remain seated during the entire traction period of three months, others may be able to walk. In both situations, traction is continuously applied. The continuous application of traction with gradual increments of traction forces results in the elongation of the entire spine, thereby providing the surgeon with a larger inter-vertebral disc-space in the scoliotic spine to increase the efficacy of the surgery. HGT also results in an increased post-operative curvature reduction[2][4][5].

HGT over a period of 10-12 weeks results in an average length increase of 76 mm from T1-S1 (which are the vertebra) as a result of HGT[2]. During this period the patient experiences several physical and anatomical changes, such as an increase in length, an increase in air volume of the lungs and a decrease in the Cobb angle. In some cases, even a few seconds after the first application of traction, the advantages are immediately noticeable in the form of an increase in pulmonary functioning for the patient. The application of HGT over a longer period of time results in an increase in Forced Vital Capacity (FVC)[2][4][6][7]. This is a huge relief for the patients who have a hard time to breathe due to severe scoliosis. Some people might find applying pins to the skull of a pediatric patient a drastic procedure. However, post-treatment experiences of these patients are surprisingly positive. The direct benefits from this procedure seem to dominate over the fear of pins clamping the skull. The pain is restricted to some headache during the first couple of days of halo application, when no other complications occur.

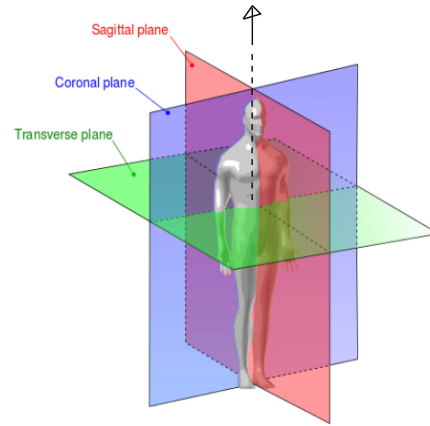


Figure 1: Force vector generated by the traction weight pointing perpendicular to the transverse plane[1].

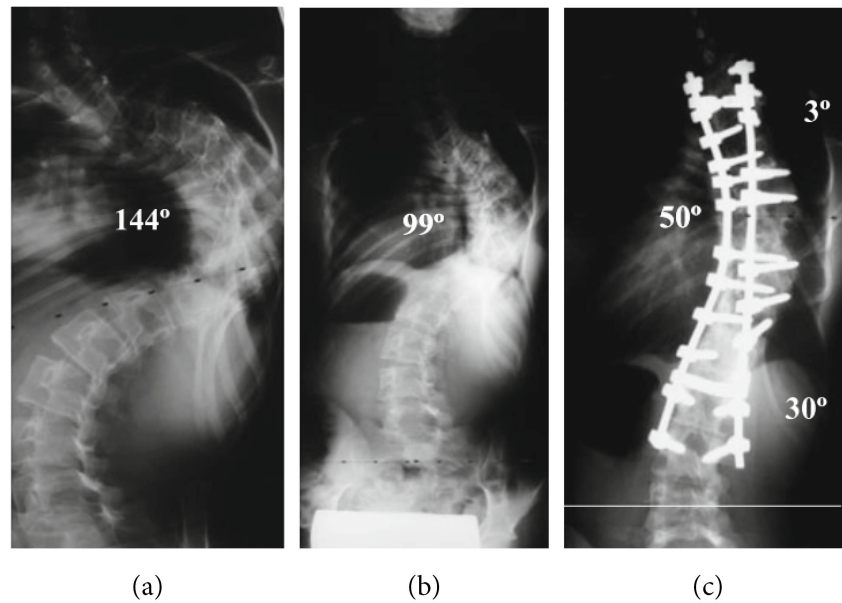


Figure 2: (a) Severe scoliosis with a Cobb angle of 144° . An 'S-shaped' curve is clearly visible in the coronal plane. (b) Reduction of the Cobb angle due to HGT pre-operative to surgery. (c) 3 year follow-up result of spondylosis. Eventually, a reduction from 144° to 50° of the Cobb angle is achieved in this example. CT images are copied from those of Watanabe et al., (2010)[2].

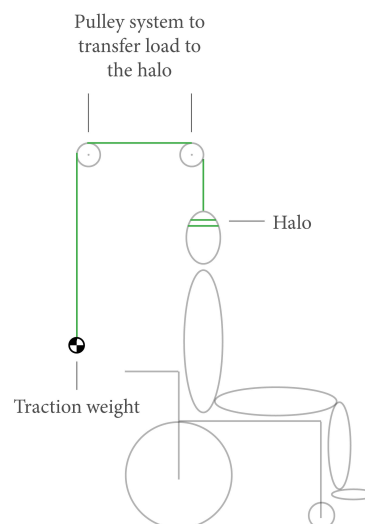


Figure 3: A schematic illustration of HGT performed on a patient in a wheelchair. The traction force is applied by adding weights. If the patient is not able to walk, he/she is in a wheelchair or in a bed. Via a mechanical system with pulleys, weight acts in the gravitational direction and is transferred to the cranium of the patient via a halo.

1.2 HGT at UMC Utrecht

The current HGT at UMC Utrecht is performed by applying traction using a Bremer halo ring, which is shown in Figure 4. The Bremer halo has a double C-shaped structure which provides the needed rigidity to the ring during HGT. Fifteen threaded holes in the ring provide the possibilities to place halo pins at the site chosen.



Figure 4: Current halo used in UMC Utrecht. Black anodized aluminum ring has several threaded holes for titanium pins to run through. The rim (grey part) is used to transfer the traction force to the ring and allows the patient to nod.

Prior to ring and pin placement, cranial anatomical landmarks are highlighted either visually, by touching and/or via CT scan. Usually patients receive general anesthesia during halo placement. Local pin placement is guided by a mark on the skin based on the global halo placement and the obtained anatomical landmarks. Hair is removed if necessary. The patient's cranial epidermis and the halo pins are disinfected. The halo pins used at UMC Utrecht are standard pins, which will be described in Section 3.5. The standardized sizes of the current rings are small (S) and large (L). If a small ring does not fit, a larger ring is needed, which results in the use of larger pins.

The pins are guided through the Bremer ring onto the surface of the cranium as shown in Figure 5. A calibrated torque screwdriver is used to tighten the pins to the prescribed amount of torque. A standardized torque value of 0.45 Nm is used to tighten several pins to the patient's skull. The number of pins is determined by the clinician. 6 pins (4 posterior and 2 anterior) are currently used as a safe standard on pediatric patients. The combination of torque and pin number is empirically determined. Each patient is assessed on his/her mental and physical condition before halo application.

The first four to five days after halo placement, no weights are added so that the patient gets used to wearing a halo. Weights are later on added to start the traction procedure, which commonly starts at 20 Newton (N) and is usually increased up to 50% of the body weight of the patient. At UMC Utrecht the usual HGT procedure consists of 10-12 weeks of HGT with bi-weekly visits to check pin site locations to detect any migration and/or infection. During this visit, the pins are re-tightened if loosening has occurred. The need for additional traction force is assessed. The majority of patients are not able to walk during this period due to their current medical and physical conditions. They remain seated in a wheelchair or a lounger at UMC Utrecht. Constructions with pulleys and weights are used to apply traction to the patient's spine during these 3 months. Upon completing HGT, the patient undergoes surgery for spondylodesis.

1.3 Problem identification

1.3.1 Improper fit around the cranium

At UMC Utrecht the standard (non-customized) halo ring sizes may result in a ring that is either too small or too large for the patient. In addition, not customized halo rings introduces not equal and sometimes large moment arms of the pins. Not equal moment arm distances lead to differences in moment at the tip of the pin causing different bone responses at the pin/skull interface. Larger moment arms lead to larger moments at the pin tip, which has been described as a factor contributing to pin loosening[8].

Furthermore, current halo rings are designed with pin positions on the forehead of the patient, leaving lifetime scars. In addition, the current rings are designed to be bulky.

Therefore, the request arose to design and develop a customized halo ring with increased patient comfort and was it desired to be designed to be less bulky.

1.3.2 Pin loosening

Pin loosening is one of the most common problems during HGT[9][10]. Loosening can cause problems such as pin-site infections and vertical migration of the halo. There are multiple causes for pin site loosening in the Bremer halo including the mechanical properties of the ring[11][12], variations in pin force applied by different clinicians during pin tightening[13], the influences of the mechanical and geometrical properties of the thread on the tightening torque[13][14][15][16], pin placement considerations[8][17][18][19][20] and the influences of geometric and geometric properties of the pediatric skull[21][22][23][24][25][26]. The solution to pin loosening is re-tightening, or complete replacement of the pin. These solutions are uncomfortable for the patient.

It is desired that the clinicians should be able to know the exact pin tip forces during HGT for the assessment of the treatment and to apply an exact known axial pin force as wished. Currently, torque is applied to the pin, which ideally should be translated to a corresponding axial pin force. However, this translation is mainly dependent on the friction in the thread and therefore an alternative solution must be sought as will be explained in detail later.

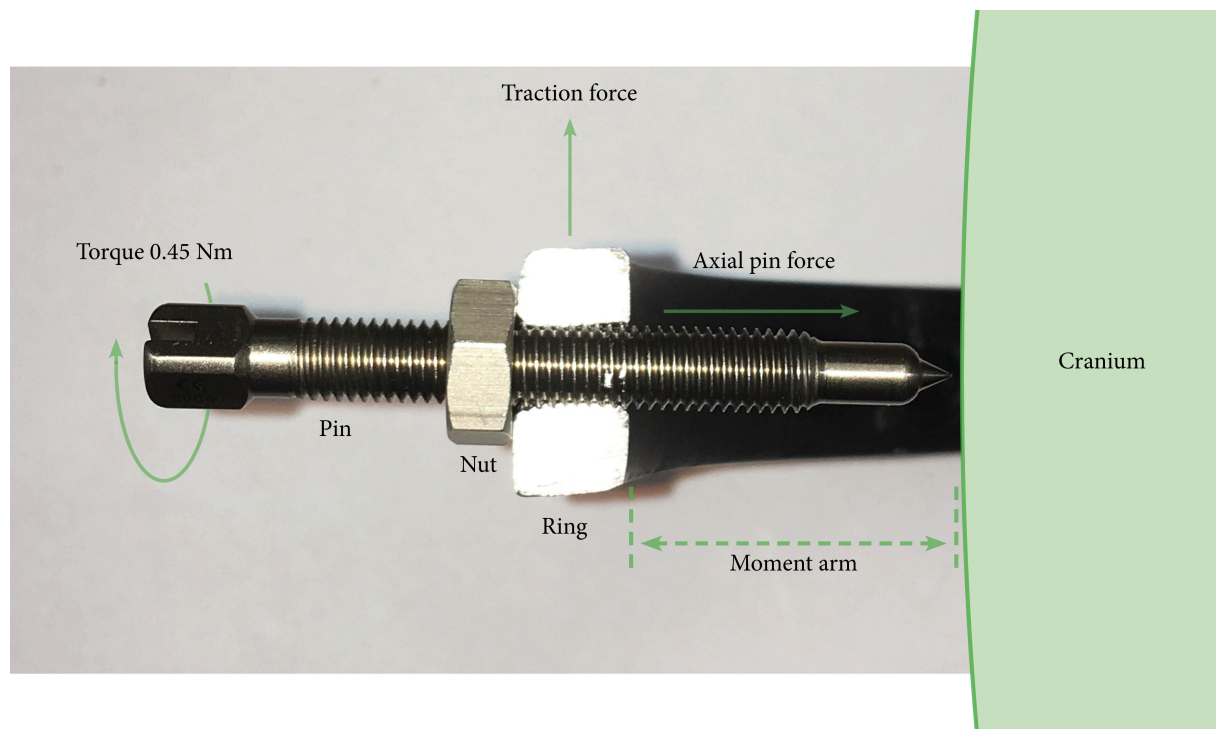


Figure 5: Overview of the main components and forces within the system of the Bremer halo ring, pin and cranium. By applying torque to the pin, an axial pin force is generated.

2 Shortcomings of the Bremer halo

In this research the Bremer halo was used as the control for comparison purposes. This research was aimed to solve or decrease some of the following limitations of this halo.

I. Improper fit around the cranium

- The ring is generalized in size (not customized for the patient)
- The pin positions leave visible scars on the forehead

II. Pin loosening

- The ring stiffness does not provide proper pin fixation (spring characteristics)
- There are undefined pin reaction forces during tightening
- Pin force is assessed by measuring torque (torque-based tightening)
- It is an over-defined mechanical system

The first five shortcomings will be discussed below and were to be solved in this thesis project. The last point remains to be addressed.

2.1 Improper fit around the cranium

2.1.1 Generalized ring

There are only two Bremer ring sizes, small (S) and Large (L), but patients have various skull geometries and sizes. This can lead to the following problems:

- Inconsistencies in the moment arms of the pins.
- A lack of control over the pin orientations with respect to the skull.

Perpendicular pin orientation improves mechanical characteristics, as compared to the placement at a deviated orientation, as shown in Figure 6[16][18][27].

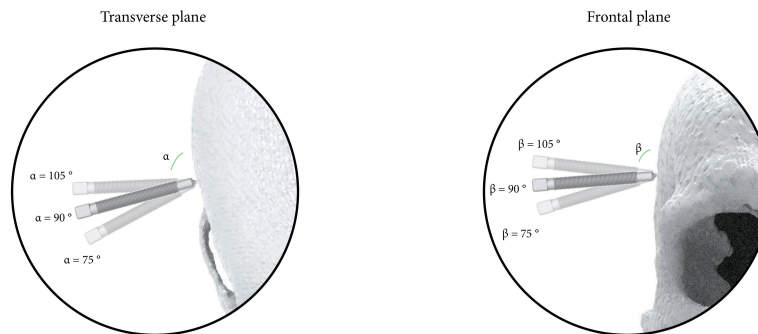


Figure 6: Orientations of more than 15° deviation from perpendicular placement to the skull leading to decreased mechanical characteristics at the pin/skull interface ($\alpha, \beta = 90^\circ$).

2.1.2 Visible scars

Currently anterior pins are placed on the forehead of the patient, i.e. in the 'safe zone', which is illustrated in Figure 7. The placement of these pins on the forehead leave unwanted visible scars[2][28]. Children who have these scars will carry them for the rest of their lives. K. Semmelink researched alternative locations for anterior pins in the temporalis region of the cranium[29].

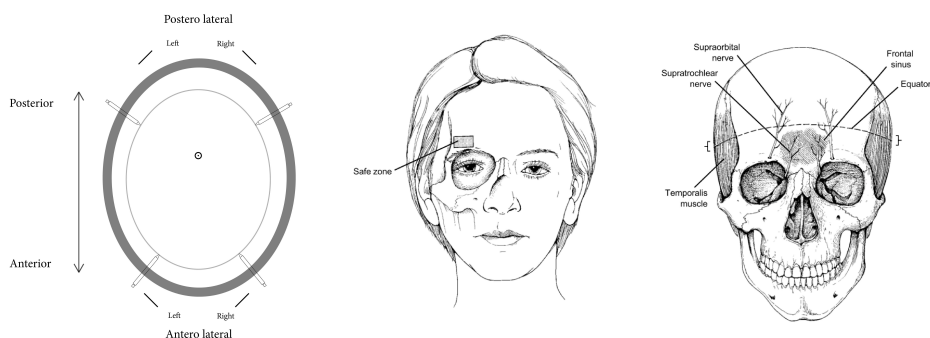


Figure 7: On the left the dark grey oval represents a closed-profile halo ring. The smaller lighter grey oval represents the cranium. The dot at the median of the cranium is roughly the position where the traction force is applied and points vertically away from the paper. The middle illustration shows the safe zone for current anterior pin positioning. On the right the most important neuromuscular sites are highlighted and should preferably be avoided when the Bremer halo systems are mounted. The middle and right illustrations are copied and slightly modified from those of Botte et al., (1996)[30].

2.2 Pin loosening

2.2.1 Spring characteristics

Halo rings are typically made of stainless steel, carbon-graphite, titanium alloys, or aluminum alloys[11][31][32]. Halo rings can be interpreted as springs with each ring having its own characteristics regarding their geometry and material. Given Hooke's law for a linear spring, the resistance to deformation is characterized by K in Equation 1, which is the spring constant.

$$F = -K \cdot x \quad (1)$$

where:

F = Force needed to stretch the spring (N)

K = Spring constant of the spring ($\frac{N}{mm}$)

x = Displacement of the spring (mm)

When tightening the pins of a halo, the reaction force at the cranium is 'spring loading' the halo ring. Young's modulus relates elongation to stress and is the stiffness of the ring material. Combined with a given geometry of the ring, the stiffness results in a resistance against deformation when the ring is subjected to a given force at a given position. The resulting deformation of the halo ring is determined by the local spring characteristics at that position.

Halos currently on the market have several shapes: commonly open C-contour, closed contour or a double C-contour (Bremer halo) (see Figure 8).

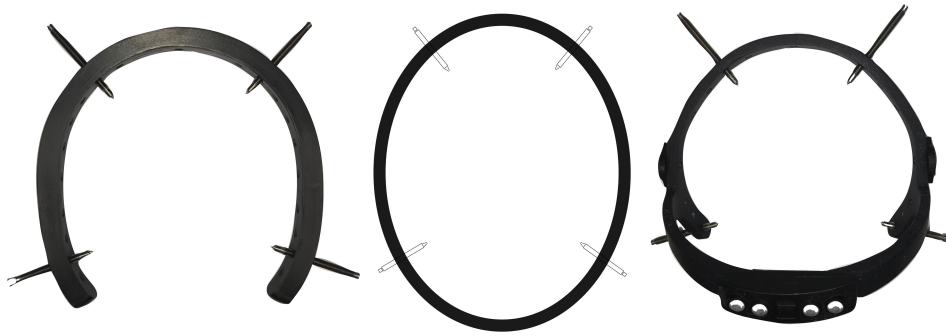


Figure 8: Current halo rings: open C-contour (left), closed contour (middle) and double C-contour (right).

These three halos shapes have their own spring characteristics at a given position on the ring. According to FEM analysis, at a force of 450 N, the anterior pins of the Bremer halo (shown on the right in Figure 8, made of aluminum) were able to displace the ring over a distance of 0.16 mm, if it was solely subjected to pure bending of the ring due to the force of the pins. In this case, the spring characteristics would reach a value up to $2812 \frac{N}{mm}$. Appendix A describes the setup and methods used for these findings.

In addition to the spring characteristics, the reaction forces due to the tightening of the posterior pins account for the total force acting on the anterior pins of the Bremer halo. 26% of the anterior axial pin force was generated by the posterior pins, as shown in Figure 11.

Bone is a living, visco-elastic material and thus it has the ability to adapt its geometry under certain loading conditions[22]. Given the characteristics of bone, geometrical changes of the skull occur when it is subjected to axial pin forces. It is believed that geometrical changes of the skull contribute to pin loosening[9][11][17][27][31]. If the anterior pins solely gain their forces due to the spring characteristics of the ring, the loss of force at these positions is very susceptible to the geometrical changes of the skull, causing the pins to loosen.

2.2.2 Undefined pin reaction forces

The Bremer halo was experimentally proven to act as an over-defined mechanical system, causing an uncertain distribution of the resulting axial pin forces during pin tightening. The experiment is described below and aimed to gain an insight into the influence of tightening a pin on the resulting axial pin forces. Then comparison was made in Section 6.2.4 to the novel halo regarding the axial pin reaction forces.

A Bremer halo was provided with specially-designed spring loaded pins. The special pins contained a spring from which the spring constant was known. The axial displacement of the pin was measured with a dial indicator, each having a standard error of 0.01 mm. The pins were connected to a piece of steel. Each pin tip fitted into a small conical hole, just as the pin would create when tightened to a bony surface[33]. Steel was used to minimize any time dependent material behavior (such as visco-elasticity). One of the pins was tightened with steps of 1 mm up to 4 mm, which was indicated by the dial indicator. Tightening to 1 mm corresponded to an approximate axial pin force of 52 N. The axial displacements of the other pins were noted and converted to force. This procedure was executed for each of the pins. It was hypothesized that tightening a pin would result in an axial pin response in all of the other pins. An overview of the setup is given in Figure 9.

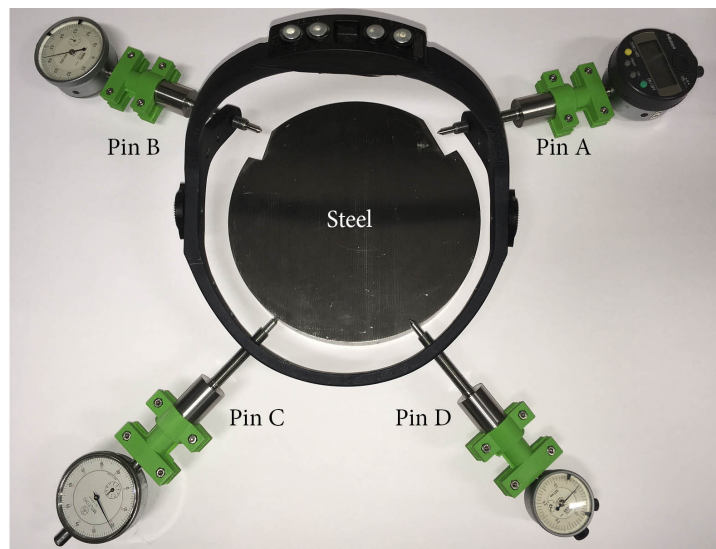


Figure 9: Test setup to determine the influence of tightening one of the pins on the axial pin forces of the other pins. The pins were equipped with an internal spring with a spring constant of $52 \frac{\text{N}}{\text{mm}}$. The green housing connected the dial indicator to the pin.

The results are shown in Figure 10. During the tests, it was found that by tightening pin A, all other 3 pins responded. Next to their response in the axial pin force, slight non-axial shifting of the tip was observed at pin D. This shifting was also observed during the tightening of pin B, on pin C. Even though the Bremer halo seems symmetric about the sagittal plane, the pin responses are not as the results of A are compared to B.

During tightening of pin C or D, only 2 of the other pins showed responses in axial pin force. However, during both of these tests one of the tips of the pins popped out completely of the conical hole during the tightening step from 208 to 260 N. During the tightening of pin C, D popped out and during the tightening of pin D, C popped out. This behavior was caused by a non-axial force vector as a result of the mutual orientations of the pins. This experiment demonstrated that the pins in the Bremer halo all influenced each other, the influence was unpredictable and non-axial pin forces were generated.

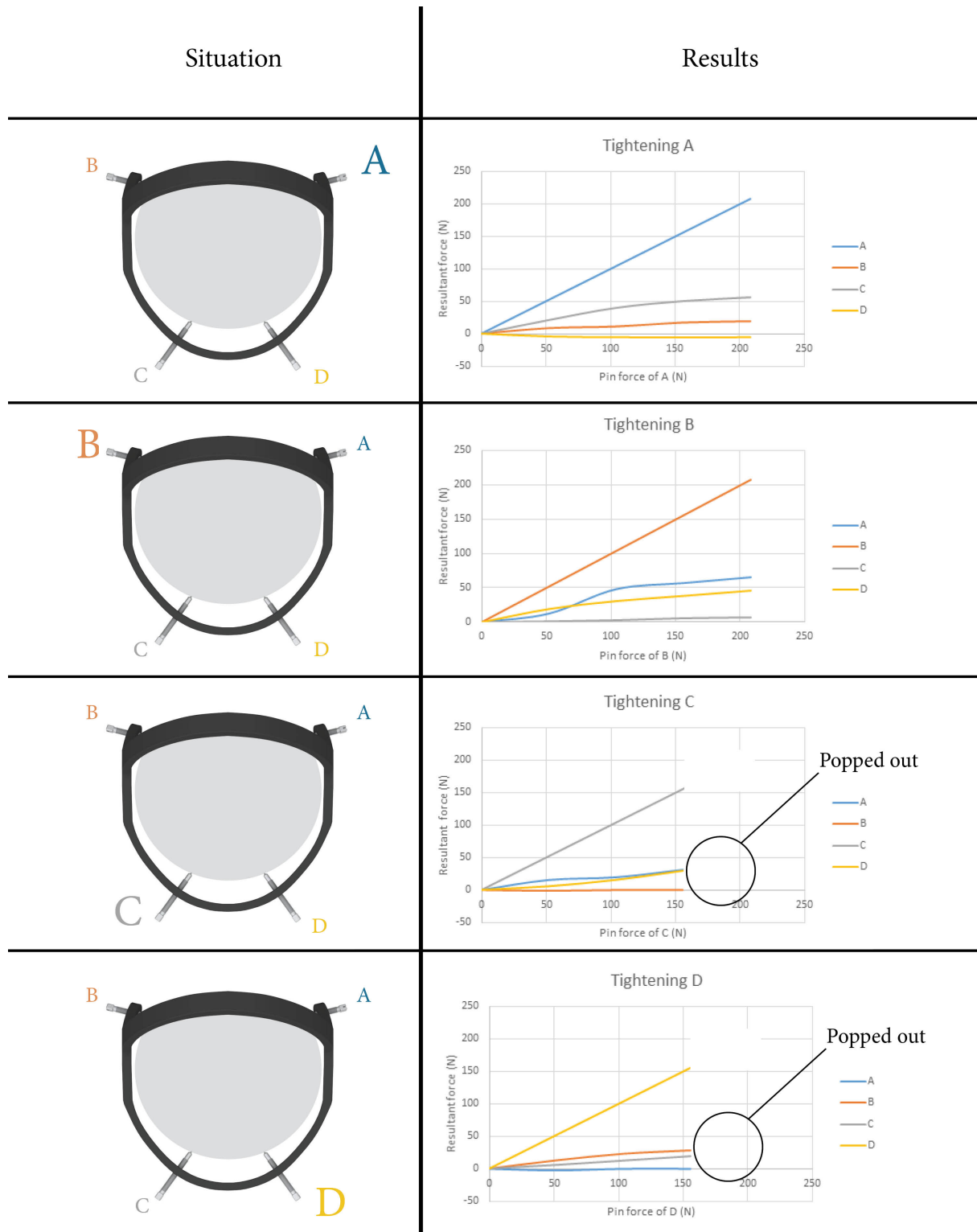


Figure 10: Responses of the over-defined mechanical system in the Bremer halo when one of the four pins is tightened. The highlighted letter represents the pin that is being tightened, corresponding to the graph on the right.

2.2.3 Torque-based tightening

Currently, the torque applied to the pin is used as an assessment to ensure that the pin is properly tightened. The torque results in an axial pin force at the pin/skull interface, which is illustrated in Figure 5.

Perra et al., (1996) established a widely accepted relationship between the amount of insertion torque applied to a pin and the loosening of this pin[13]. Higher torque would result in a higher axial pin force which should have improved mechanical locking of the pin to the skull. Whitesides et al., (1992) reported a large variety of pin tip forces between halo systems, when tightening a pin with a certain amount of torque[34]. For example, a torque of 0.45 Nm applied to a steel halo resulted in an average axial pin force of 212 N, while the same torque applied to a nylon and fiberglass halo resulted in an axial pin force of 578 N. Even though the same halo system was used, tightening variances between clinicians would not reliably achieve the same torque, as demonstrated by Smith et al., (1996). Additionally, the tools used to apply torque were not consistent, as observed by Smith et al. The tools used in UMC Utrecht were recorded to have an accuracy of 61%[13].

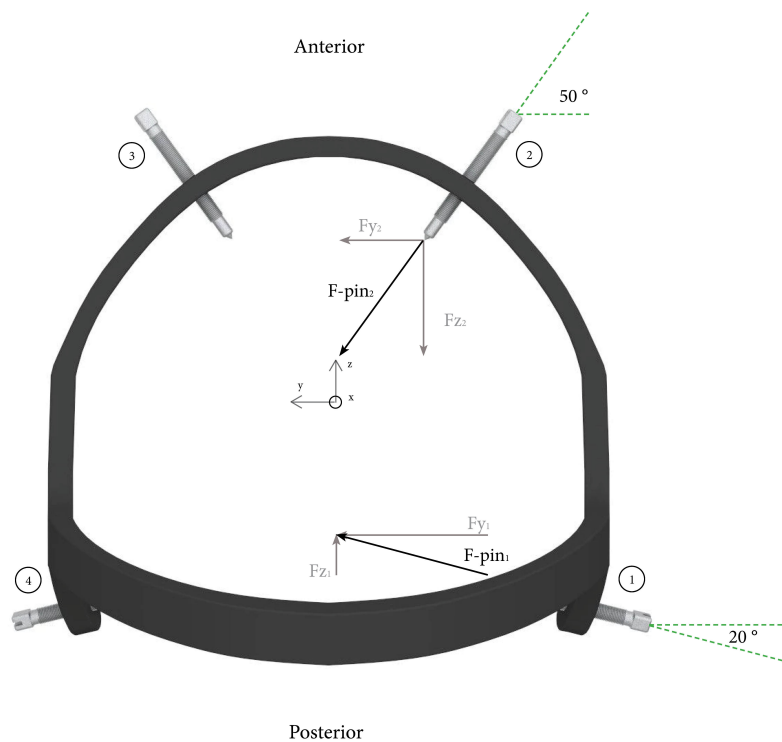


Figure 11: Orientations of the anterior and posterior pins of the Bremer halo ring. If one of the posterior pins is tightened, naturally reaction forces on the other pins are generated. In this example 26% of $F\text{-pin}_2$ will be generated by $F\text{-pin}_1$. The mutual orientation of the pins causes additional friction in the thread due to non-axial pin forces.

The pins in the Bremer halo are diagonally tightened, meaning that pins 1 and 3 are a pair, just as pins 2 and 4 as shown in Figure 11. This clinical standard procedure (as well as other tightening configurations) naturally introduces non-axial forces to each pin (e.g., F_{z2}). At the pin/thread interface, non-axial pin forces result in a pin being slightly crooked in its thread, resulting in additional friction during tightening, as shown in Figure 12. Consequently, a given torque does not result in an expected axial pin force of the pin anymore. In other words, torque introduces a large variety of axial pin forces during tightening. By having no control over the axial force of a pin, no insights into the static mechanical system of the halo and pins can be obtained. These insights are however needed to assess the functionality of the halo, regarding pin loosening. Therefore, an alternative way of applying force to the pins was explored in this study.

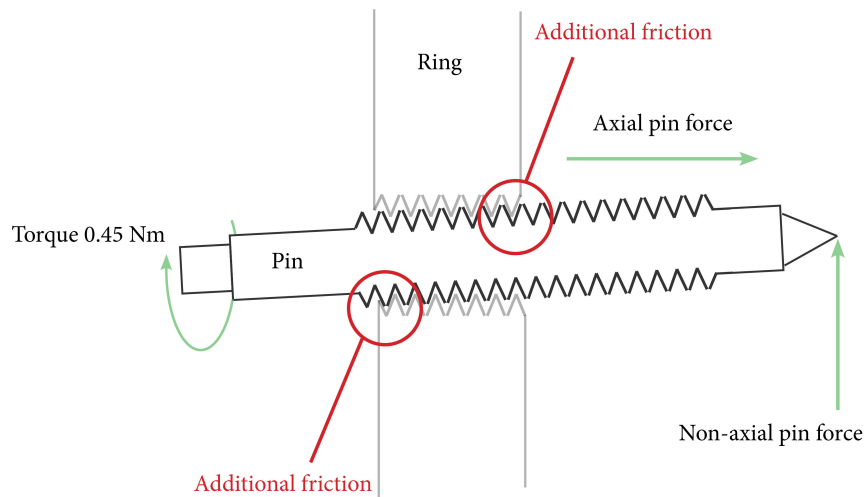


Figure 12: Top view. A non-axial loaded halo pin will cause additional friction in the thread. Torque is related to the axial pin force via the friction and therefore this situation will lead to a lower axial pin force at a given torque.

3 Novel halo

3.1 General objective

The request of UMC Utrecht, combined with the shortcoming issues of the current Bremer halo used during HGT treatment, led to this research. The general objective was to design, produce and test a patient-specific halo, with which the degradation of the axial pin force over time could be measured by the displacement of the ring at the pin site location. The first step was taken to custom-design the patient-specific geometry of the halo and also to design the stiffness of the ring at the pin site location. By doing so, the displacement at the pin sites causes controlled degradation of the axial pin force over time and pin loosening can be prevented.

This research was aimed to solve the current shortcomings of the Bremer halo by proposing the following solutions:

I. Customization

- Customized ring size and geometry
By designing a customized halo ring, the moment arm at all pin site locations can be kept consistent. Furthermore, the pins can be oriented perpendicularly to the surface of the skull. The distance between the skin of the patient and the ring should still be enough to allow proper cleaning, which is approximately 20 mm[35].
- Novel anterior pin locations
A novel pin location can be introduced so that the scars on the forehead will not be visible anymore.

II. Axial pin force control

- Customized ring stiffness
By designing a halo ring with a suitable stiffness at the pin site locations, the pins should be able to maintain their axial forces even though the skull might change its geometry over time.
- Well defined pin reaction forces during tightening
By designing a halo with two separated C-contours during tightening, the pins will only influence their opposing pins instead of all the other pins. By doing so, an improved assessment of the pin force during tightening can be obtained.
- Pin force assessed by displacement
Applying force to the pins is based on measuring the displacement of the ring. By knowing the stiffness of the ring at a particular position and the ring displacement, the force can be derived.

3.2 Design process

In cooperation with the clinicians at UMC Utrecht, a list of requirements were determined for the novel halo, which are given in Appendix B. During expert meetings, these requirements were discussed, as well as partial solutions to partial problems, which are given in Appendix C. After proposing several concepts, a decision was made on the final concept which each expert agreed upon.

A fresh frozen male human cadaver head was Computed Tomography (CT) scanned and used to obtain the skull geometry data as shown in Figure 13. The reconstruction of the facial skin was made, solely for visual purposes. The thickness of the skin was assumed to be 5 mm. The radiation dose during CT was 4 millisievert (mSv).

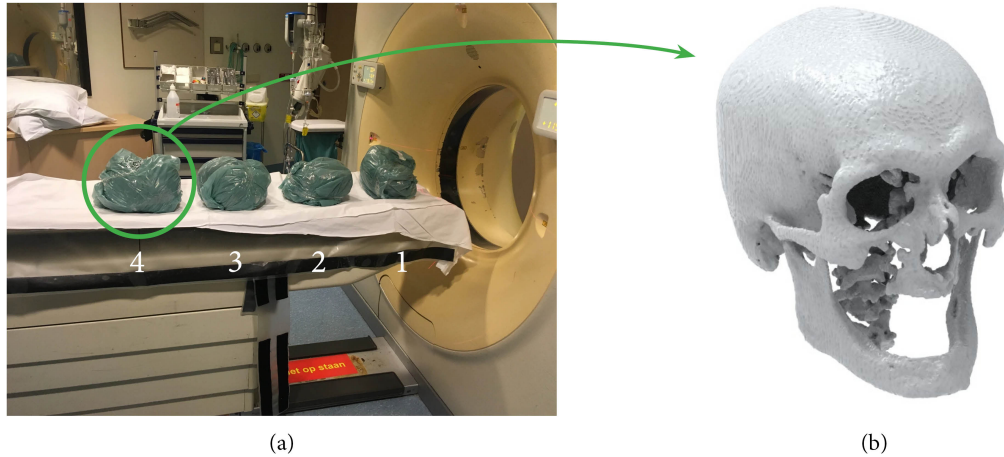


Figure 13: (a) 4 fresh frozen cadaver heads subjected to CT scan. Head number 4 was used for the customization of the halo ring. Heads 1,2 and 3 were used by K. Semmelink for his research. (b) STL file imported into Solid Edge ST 10, converted from the CT image.

The CT images from the fourth skull in Figure 13 were loaded into the program ITK-SNAP, with which the CT data could be segmented. The segmented data was then loaded into Matlab R2017b where it was translated from pixels to millimeters. Matlab was used for converting the data to a Surface Tessellation Language, commonly known as an STL file (for the details on conversion from CT to STL please refer to K. Semmelink, who performed the conversion). This file was loaded into the 3D modeling software Solid Edge ST 10. With the geometry of the skull acquired, a model for the new halo was generated, based on the pre-defined requirements. The moment arms, pin positions and pin orientations were used as input parameters to create the 3D halo model.

The basic working principle of the novel halo was that the stiffness of the ring at the pin locations was custom designed. The axial pin force was generated by combining this stiffness with a displacement induced by tightening, as illustrated in Figure 14.

The spring stiffness of the ring met the requirement of a maximum displacement of 5 mm at each pin site location (one side of the skull), which was based on the knowledge and experience of Dr. M. Kruijt and confirmed by the validation of the 3D-model of the skull in CAD. Currently, a torque of 0.45 Nm is used to tighten the pins to the skulls of pediatric patients. A study conducted by Whitesides et al., (1992) showed that 0.45 Nm could result in a maximum axial pin force of 450 N[34]. According to the analysis presented in Appendix E, the axial pin forces created by the Bremer halo in a test setup (not in a clinical setting) would reach values up to 395 N, when a torque of 0.45 Nm was applied, which made the findings of Whitesides et al., plausible[34]. The spring characteristic was determined by the geometry and material properties of the C-contours. A spring characteristic of $45 \frac{N}{mm}$ was assigned to the novel halo. The methods to obtain the spring characteristic in Solid Edge ST 10 are listed in Appendix D.1.

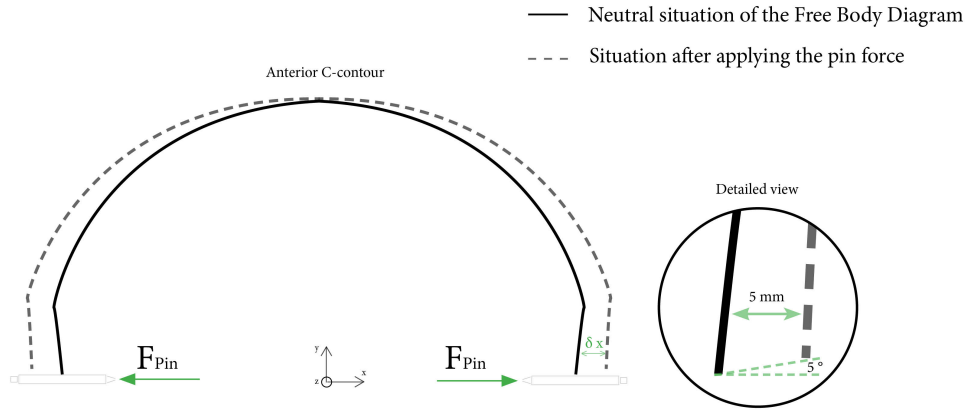


Figure 14: Working principle of a C-Contour. Displacement is initiated by tightening. In combination with the stiffness of the C-contour, the force can be derived.

After producing both C-contours, the stiffness values were checked and turned out to be $55 \frac{N}{mm}$ and $44 \frac{N}{mm}$ for the anterior C-contour and posterior C-contour, respectively. These findings are described in Appendix D.3. The deviations in stiffness between the 3D-model and actual values can have multiple reasons:

- A variation in geometry between the model and actual C-contour
- A difference in Young's Modulus between the theoretical value and actual value
- The orientation of the part in an SLS machine.
- The position of the part in an SLS machine.

By tightening the pins to a right amount of force, the distance between the epidermis and halo ring reaches a value between 15 and 20 mm, which allows for cleaning, since the C-contours will be able to move a few millimeters as a response to pin tightening[35].

3.3 Anterior pin location

The wish to change the anterior pin location from above the eyebrows to a location at the hairline led to the research of K. Semmelink. He examined the possibility of placing an anterior pin in the region of the musculus temporalis. Pins were placed at different positions in the musculus temporalis region. A traction force was applied to the pin. The force was increased until the pin lost grip and started to migrate in the direction of the force. This test was performed at different axial forces on the pin at different locations in the assigned region. The results showed that with an axial force of 150 N on a pin, a traction force of at least 200 N could safely be applied, before the pin started to migrate along the surface of the skull and the applicable traction force was independent of the location at the musculus temporalis region. A linear relationship was found between the axial pin force and the maximum traction force.

For the design of the novel halo, a maximum pin force of 450 N was initially used as input and 200 N as the minimum required axial pin force to perform traction to 200 N[27]. During the design the halo, no results were published yet by K. Semmelink and therefore could not yet be used. The blue area in Figure 15 indicates the region where the anterior pin could safely be placed.

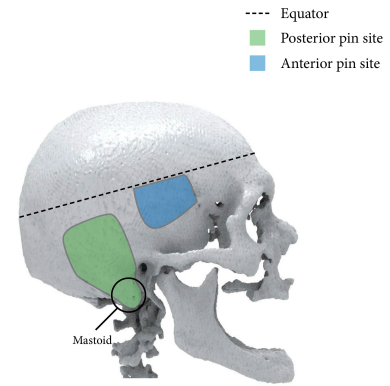


Figure 15: Novel anterior pin placement indicated by the blue area in the musculus temporalis region and the posterior pin placement indicated by the green area at the mastoid region.

3.4 Posterior pin location

Currently, the posterior pins are preferably placed in the region of the mastoid of the skull, as indicated by the green area in Figure 15. The mastoid is generally a thick part of the skull. The placement of the posterior pins is less critical, as compared to the current anterior positioning due to the absence of important muscles and arteries in this region[30]. For the positioning of the posterior pins (and also the anterior pins), it is important that these are positioned below the equator of the skull, which is the area of the largest circumference[30].

3.5 Pins

Considering the preference of UMC Utrecht, commercially available pins with a conical pin tip were used. These pins were partially threaded and provided with a nut, as shown in Figure 16. The thread is $\frac{1}{4}$ inch UNF (Unified National Fine thread). The manufacturer provides pins with a variety of axial lengths varying from 60 mm to 75 mm. The pins are made out of titanium.

The conical shape of the tip of the pin is designed to increase the surface area when it slightly penetrates into the outer layer of the skull. After the conical pin tip, the pin gets even thicker which is designed to prevent complete penetration. Plastic deformation of the skull ensures an increased surface area of the tip of the pin and thus a decreased pressure at the pin/skull interface[33].



Figure 16: One of several pins used to lock the halo to the skull. The tip of the pin is pressed into the skull of the patient.

3.6 The novel halo

Figure 17 shows the novel halo with numbered parts. Table 1 lists these parts, their materials, production methods, features and functions. To attach the halo to the patient, part no. 3 will be put on the epidermis and held in position. Parts 1, 2 and 4a will be placed onto 3 with the bows of 1 and 2 opposing each other (as shown in detail on the bottom right of Figure 17). The connection for the traction rim (5) is placed over the corresponding holes in both C-contours. The pins (9) are tightened with the nut (10) already attached to the pins. Both ends of the C-contours are tightened to a right amount of displacement (which can be measured using e.g., a caliper) and thereafter 4b is connected to 4a and tightened with two bolts (6). Now part 3 can be removed and the traction rim (7) is attached to 5 with two bolts (8).

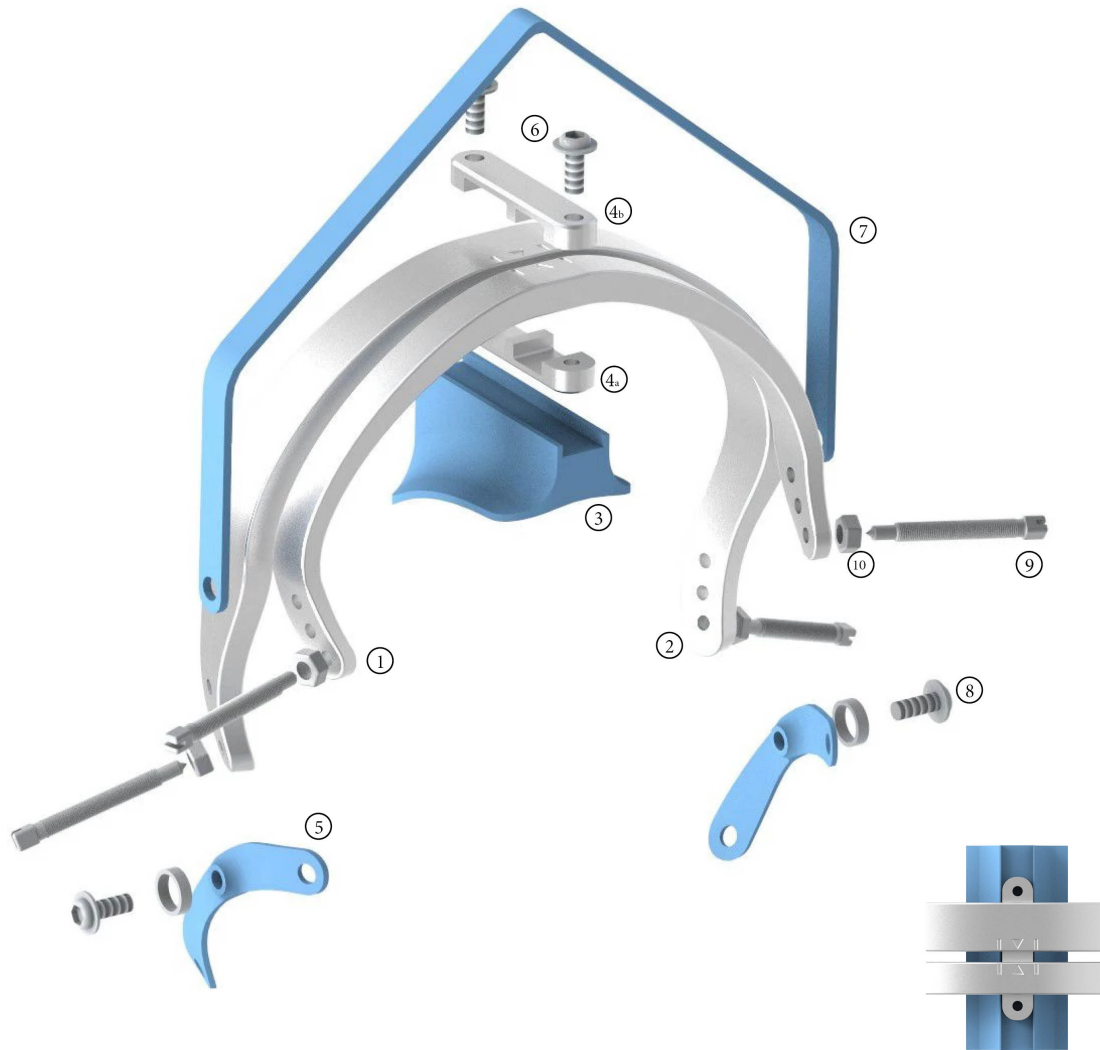


Figure 17: Illustration of the novel halo. Parts are numbered and listed in Table 1. The bottom right illustration is a detailed view on top of both C-contours (composed of parts 1, 2, 3 and 4).

Part No.	Name	Material	Production methods	Features and functions
1	Anterior C-contour	AlSi10Mg	Selective Laser Sintering	Custom designed part, contains 3 holes on each side for flexible pin locations
2	Posterior C-contour	AlSi10Mg	Selective Laser Sintering	Custom designed part, contains 3 holes on each side for flexible pin locations
3	Position block	PLA	Fused Filament Fabrication	Provides a correct height for positioning the entire halo
4a	Connection block bottom	Stainless steel	Milling	Provides relative anterior/posterior position for both C-contours
4b	Connection block top	Stainless steel	Milling	Locks both C-contours in combination with connecting block bottom
5	Connection for traction rim	ABS	Fused Filament Fabrication	Provides an interface for the traction rim to apply traction force
6	Bolt (M6 x 20)	stainless steel	N.R.	Locks the traction rim to the connection block (both 4 and 5) and C-contours
7	Traction rim	Aluminum	N.R.	Interface for applying traction
8	Bolt (M6 x 20)	Stainless steel	N.R.	Connects the traction rim to the halo
9	Pin	Titanium	N.R.	Locks the ring to the head of the patient
10	Nut	Stainless steel	N.R.	Prevents the pin from loosening

Table 1: Details of the numbered parts shown in Figure 17 (N.R. = Not Relevant).

4 Research

The overall research design and flowchart of this study is shown in Figure 18. The dotted line divides the chart into two blocks. The design process is not described in detail in this thesis, however Appendix B and C are derived from the design process and provide indispensable input data. The shortcomings of the Bremer halo are shown in the flow chart. Two out of the shortcomings (i.e., the anterior pin location and torque-based tightening) are already solved in the novel halo design. The solutions to the remaining three shortcomings were validated by conducting the following experiments:

1. **The application of the novel halo to the cadaver head.** The deviations of some intended parameters were analyzed. Some other quantifiable parameters from the Bremer halo, such as the moment arm and pin orientation, were compared to those of the novel halo to show whether customizing indeed led to any improvements.
2. **Analysis of the cadaver head.** It was believed that the visco-elastic properties of the human skull caused the degradation of pin force over time. To get an impression about how these properties would influence the axial pin force, analysis of the cadaver head with the novel halo was performed. Based on the results, predictions of the residual axial pin forces were made.
3. **Pin reaction forces.** All the pins of the Bremer halo influenced each other during tightening and non-axial pin forces were present. The tightening characteristics of the novel halo were analyzed so that the influence of one pin on other pins could be mapped. Also the influence of the bridge connector on the axial pin force was analyzed for future designs. An improvement in a more predictable pin behavior were achieved by comparing the pin behavior to that of the Bremer halo.

These three tests were divided into two parts in this research. Part I: *Customization* contains test 1 and Part II: *Axial pin force control* contains tests 2 and 3.

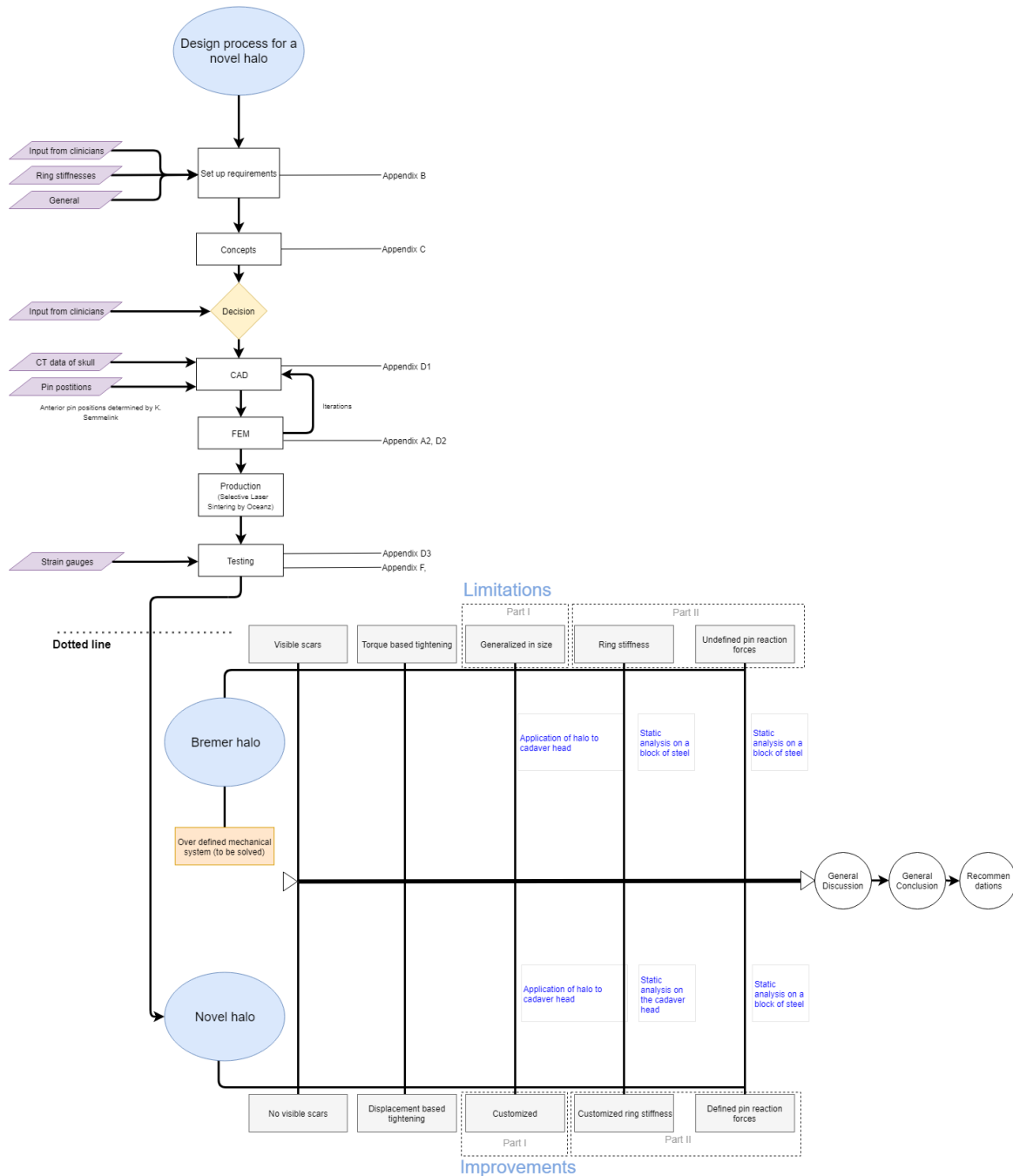


Figure 18: Steps taken in the design process to develop a novel customized halo ring. The dotted line indicates the point at which the product was finished and ready for testing.

5 Part I Customization

Two experiments were performed:

- **Experiment 1:** The moment arms and pin orientations of the Bremer halo were compared to those of the novel halo.

Comparison was made between the Bremer halo (the large variant, which was used as control) and the novel halo regarding the length of the moment arm and the pin orientation on the cadaver head. Pin position was left out, since the novel halo had new pin positions and therefore no useful comparison could be made to the Bremer halo.

- **Experiment 2:** Comparison was made between the intended moment arms, pin orientations and pin positions of the CAD model the measured values.

The pin orientation being perpendicular to the skull, as well as in the transverse and coronal planes, is believed for the halo to have improved mechanical characteristics (see Figure 21). Customizing halos brings the opportunity to determine the length of the moment arm, pin position and the pin orientations. Since this was the first attempt to create a customized halo, the deviations and limitations of the procedure should be established in order to determine its validity.

5.1 Methods

The cadaver head was partly scalped to reveal the skull and Meatus Externus (ear canal). A stroke of skin on top of the head was left over for realistic positioning, as would be done during clinical application. Both halos were mounted on the skull. An overview of this setup with both the Bremer and novel halo mounted is given in Figure 19.

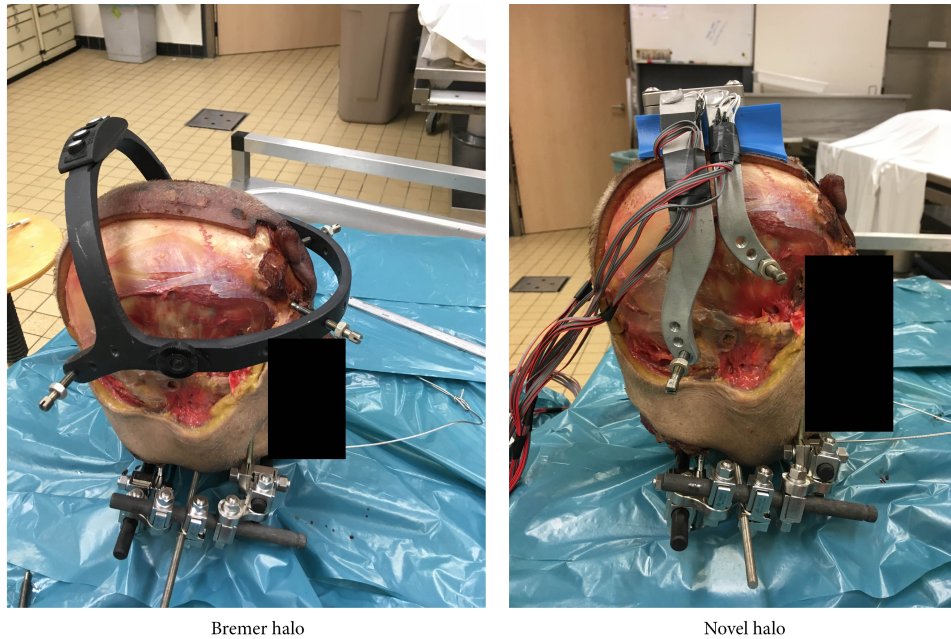


Figure 19: Both the Bremer halo and novel halo were mounted on the same cadaver head and compared with respect to moment arm and pin orientation. This setup for the novel halo was also used to determine the validity of the procedure from CT to reality.

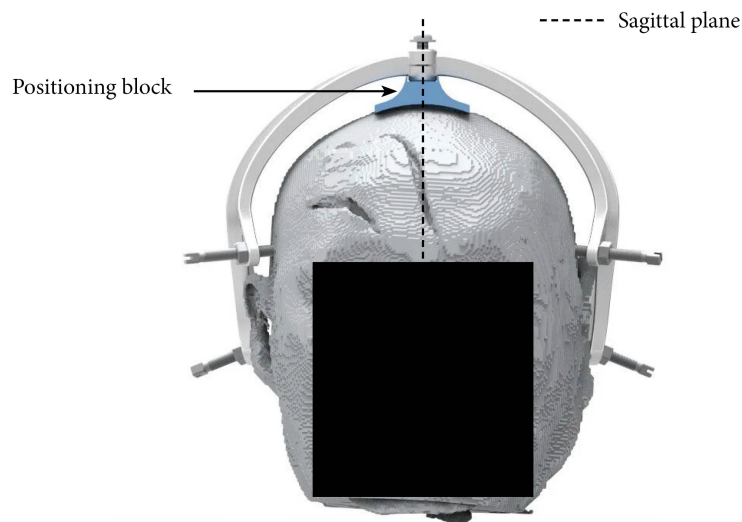


Figure 20: During the experiments the block should be positioned as symmetrical to the sagittal plane as possible.

Experiment 1

The Bremer halo was attached to the cranium of the cadaver head and the moment arms and pin positions were measured. The moment arm was measured using a caliper. The pin orientations were measured using an imaginary tangential line to the surface of the skull, as illustrated in Figure 21(a). The Bremer halo was then removed and the novel halo was attached to the cranium of the cadaver head. It was expected that the novel halo would show more consistent moment arms and pin orientations closer to the perpendicular orientation.

Experiment 2

The novel halo was positioned 5 consecutive times on the cadaver head, while each time all components were disassembled as if it was a new application of a halo on another patient. After positioning, the orientation, position and moment arm of each pin were noted. Since the position and orientation were hard to determine directly during this experiment, pictures were taken from which data was translated and converted to interpretable results.

Pin orientation was measured by the same way as described in Experiment 1. The positions were measured from the Meatus Externus (used as the origin) and expressed as the Y- and Z-coordinates. These coordinates were later on visualized on the 3D model of the skull. The distance from a data position (blue dot) to the intended position (black dot) was measured (see Figure 24). The X-coordinate was represented by the length of the moment arm and measured with a caliper. The data was compared to the same data obtained from the 3D CAD model in Solid Edge ST 10.

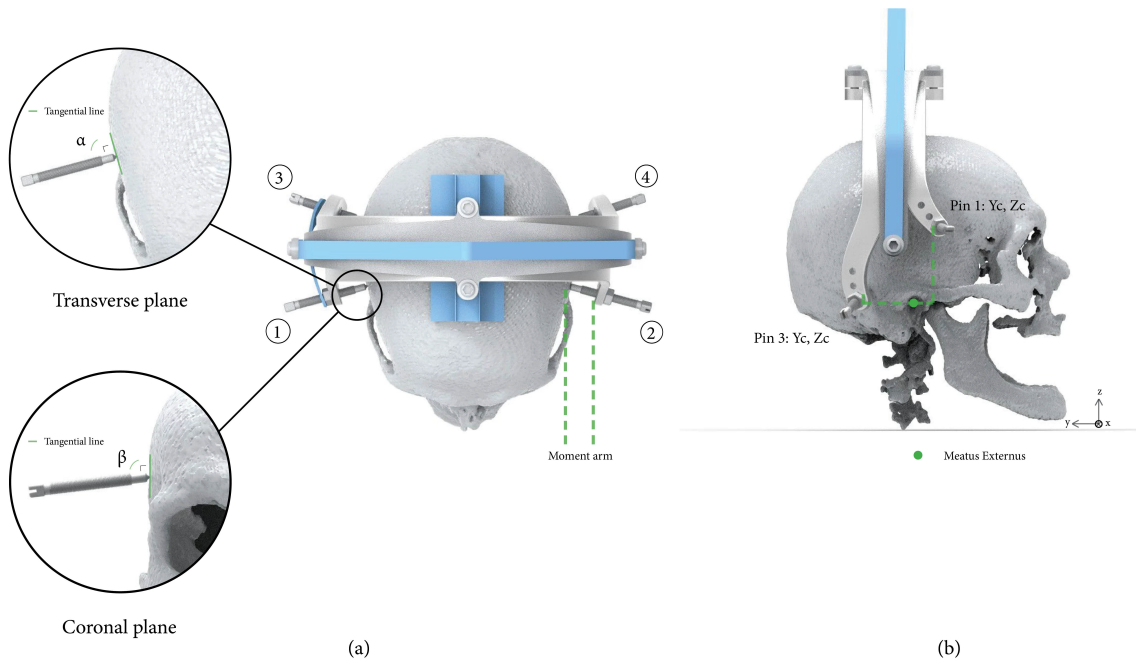


Figure 21: (a) All four pins were analyzed on their moment arms, positions and orientations. The orientation was measured relative to the transverse plane as well as to the coronal plane. A tangential line was drawn at the pin skull interface, from which the angles were measured. Note that β was initially not 90° , but shall become 90° during pin-tightening, which created a movement of the C-contour by 5° according to FEM. This was only valid for the novel halo. (b) The positions of the pins were determined with respect to the Meatus Externus. This reference point was used, as it was recognizable during the tests in reality.

5.2 Results

5.2.1 Experiment 1

A clear difference in the moment arm of each pin was found between the novel halo and the Bremer halo. The results are summarized in Figure 22. The moment arms of the novel halo remained almost the same (a maximum difference of 1 mm), while a difference of 8 mm was found in the Bremer halo. The novel halo demonstrated a smaller average moment arm of 19 mm compared to 25 mm of the Bremer halo.

The α -angle differed between -2° to $+4^\circ$ from the intended value for the novel halo and between -7° to $+2^\circ$ for the Bremer halo. Both α -angles were compared to the intended 90° .

For the β -angle the novel halo differed between -3° to $+5^\circ$ from the intended 95° . The β -angle of the Bremer halo differed between $+2^\circ$ to $+17^\circ$ from the intended 90° . The β -value for pin 1 of the Bremer halo was the only value that was above 15° . Steps of 15° are commonly used in the studies on the effect of angled pin insertion vertical pin migration. The β -values of the novel halo did not reach a difference of 15° . Due to the small sample size of the experiment no statistical relevance could be obtained from this data. However, the moment arms of the novel halo indeed showed a higher consistency and were on average 5 mm smaller than those of the Bremer halo. Both α - and β -angles of the novel halo had values approaching perpendicularity more closely than those of the Bremer halo.

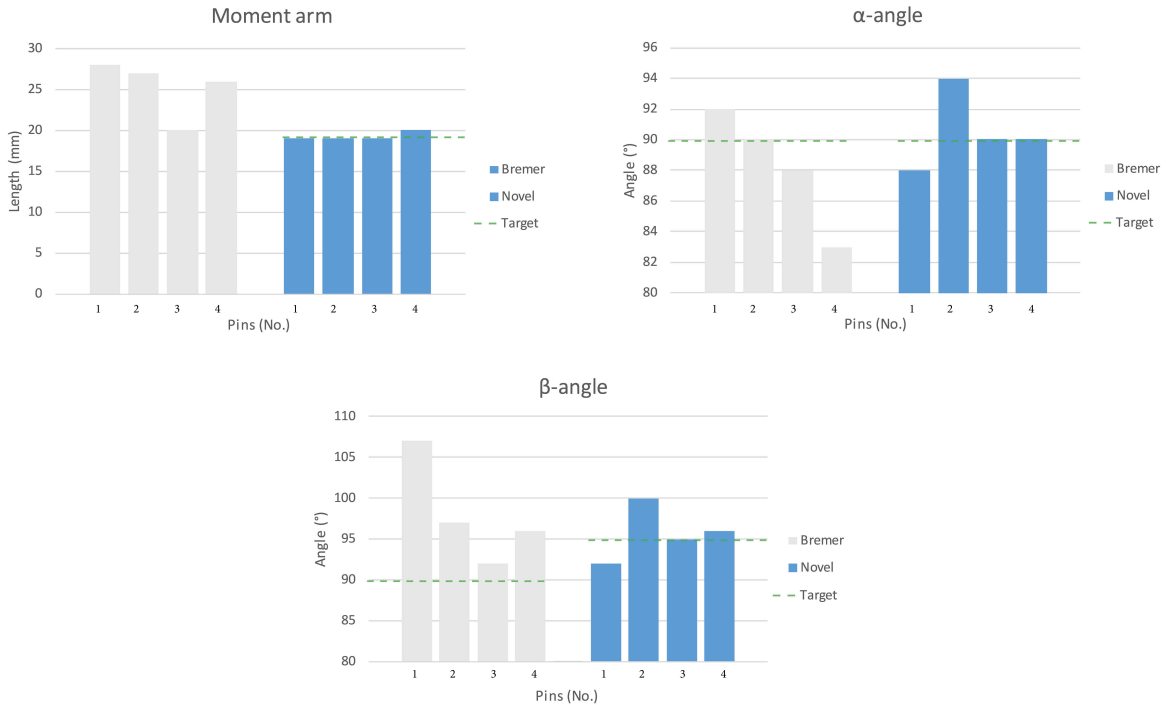


Figure 22: Moment arms and pin orientations of the Bremer halo (grey) and the novel halo (blue). The pin numbers of the Bremer halo correspond to the numbering illustrated in Figure 23. Note that there is no target value for the moment arm of the Bremer halo.

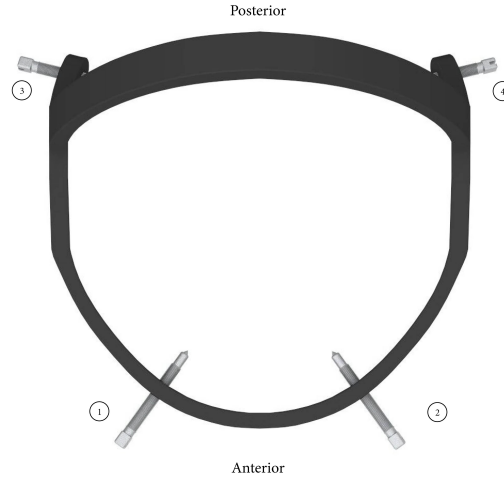


Figure 23: Numbering of the pins of the Bremer halo used during this experiment.

5.2.2 Experiment 2

Table 2 summarizes the data points at the four pins of the 3D CAD model. Data was rounded up to whole decimals. The moment arms in the model were equal for each pin. It was found that the Y_c and Z_c values were the same for pins 1 and 2. This was also the case between pins 3 and 4.

The intended value of α and β were 90° and 95° , respectively.

Pin No.	Moment arm (mm)	Y_c (mm)	Z_c (mm)	α ($^\circ$)	β ($^\circ$)
1	19	-11	55	91	95
2	19	-11	55	90	96
3	19	32	12	89	95
4	19	32	12	90	96

Table 2: Control values of the moment arms, pin positions (Y_c and Z_c) and pin orientations (α and β) of the pins of the novel halo with respect to the skull in CAD.

Reality. Over five consecutive times, the novel halo was mounted on the cadaver head. Table 3 summarizes the results obtained. Figure 24 visualizes the spread of the data points in pin position and angle. For the Y- and Z-coordinates all data points were visualized, but for α and β only the maximum values.

The standard deviations and mean values were calculated and are shown in Table 4. The distance shown in Table 4 was calculated from the Y_c and Z_c coordinates shown in Table 3.

The data of the moment arm, α and β angles were reproducible and within an acceptable range around the intended positions. The maximum deviations from the 90° α -angle found in the transverse plane were between -2° and $+6^\circ$. There have been no reported studies on the effect of pin orientations deviating from 90° over a range smaller than 15° . The deviations found in β were slightly larger than those in α (-5° and $+6^\circ$), but still remained below a difference of 15° .

The data of the distance showed an average of approximately 7 mm from the intended position, with a standard deviation of 4.4 mm. The positions of pins 2 and 4 were less accurate and precise compared to the positions of pins 1 and 3 (as observed in Figure 24). The process from modeling to evaluating a halo involved a lot of factors which could have introduced variances. The factors will be discussed in Section 5.3. The variances were most likely caused by human factors during assembling the halo to the cadaver head, since the halo itself was not disassembled during the test and the cadaver head remained at its position.

Pin No.	Moment arm (mm)	Y_c (mm)	Z_c (mm)	α ($^\circ$)	β ($^\circ$)
1	17	-11	55	90	90
2	17	-20	55	92	89
3	17	29	13	90	95
4	19	45	14	91	97

(a) Positioning 1

Pin No.	Moment arm (mm)	Y_c (mm)	Z_c (mm)	α ($^\circ$)	β ($^\circ$)
1	19	-7	55	92	93
2	19	-24	51	92	90
3	19	32	14	89	99
4	20	20	14	88	96

(b) Positioning 2

Pin No.	Moment arm (mm)	Y_c (mm)	Z_c (mm)	α ($^\circ$)	β ($^\circ$)
1	21	-11	53	92	92
2	19	-23	53	90	99
3	22	28	15	91	95
4	20	20	13	90	96

(c) Positioning 3

Pin No.	Moment arm (mm)	Y_c (mm)	Z_c (mm)	α ($^\circ$)	β ($^\circ$)
1	21	-13	52	94	93
2	19	-20	57	91	97
3	19	28	11	91	100
4	19	22	16	90	95

(d) Positioning 4

Pin No.	Moment arm (mm)	Y_c (mm)	Z_c (mm)	α ($^\circ$)	β ($^\circ$)
1	20	-8	53	90	94
2	19	-20	56	96	101
3	19	30	13	90	93
4	19	24	13	89	99

(e) Positioning 5

Table 3: Five consecutive measurements after mounting the novel halo on the cadaver head. Data was rounded to whole decimals.

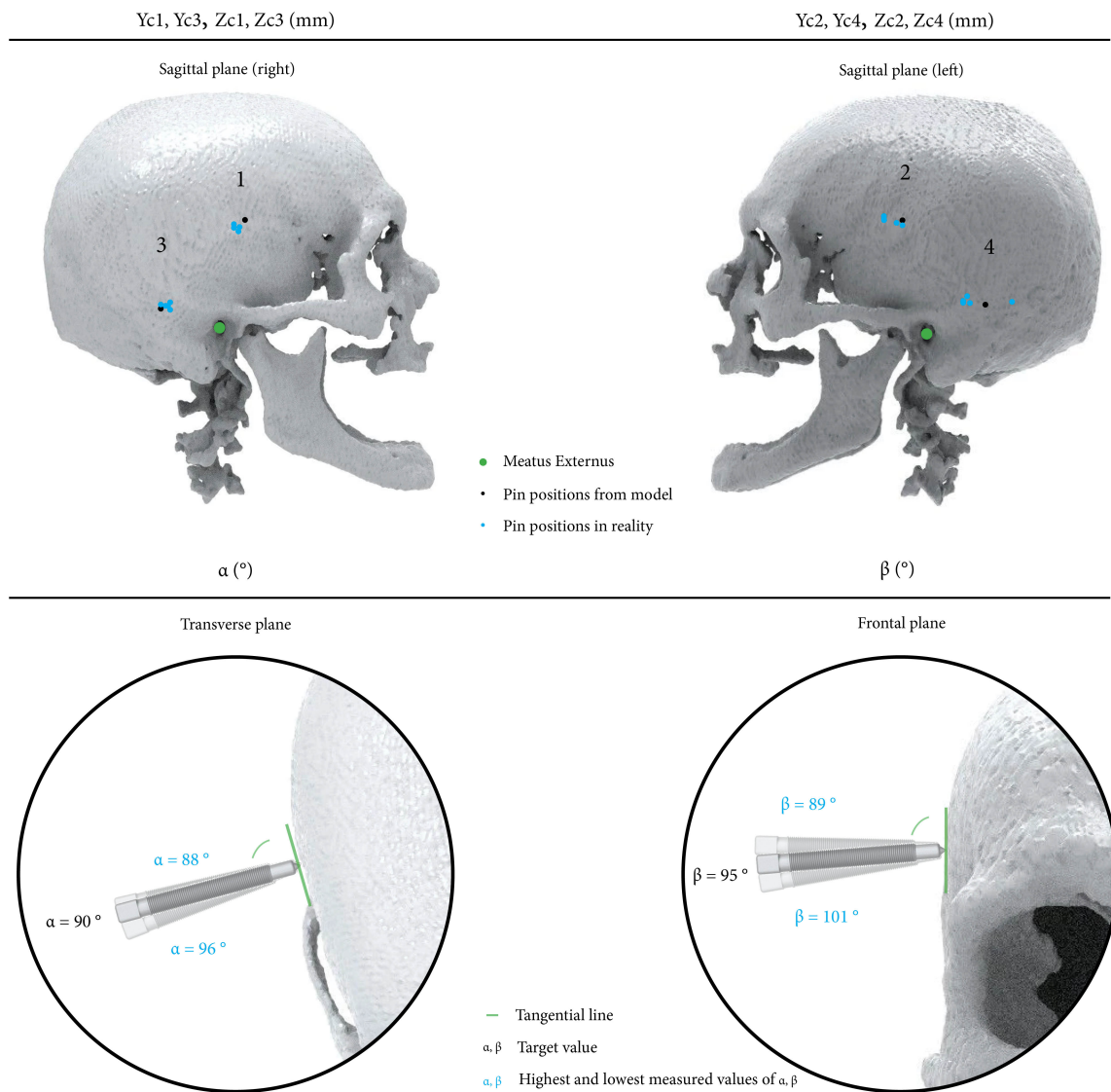


Figure 24: Visualization of data obtained from Table 3: Y_c , Z_c , α and β . All positions of Y_c and Z_c are visualized, while for α and β only the maximum values are displayed.

	Moment arm (mm)	Distance (mm)	α (°)	β (°)
Intended value	19	0	90	95
Mean $\pm \sigma$	19.2 ± 1.3	6.9 ± 4.4	90.9 ± 1.8	95.4 ± 3.3
Min, max	17, 22	0, 13.6	88, 96	89, 101

Table 4: Summary of the data from Table 3. The offset between the mean and intended value is a measure for the accuracy. The standard deviation is a measure for the precision.

5.3 Discussion

The measurements performed were derived from pictures, since direct measurement on the cadaver head turned out to be too difficult. As a result, human error could have been introduced during the generation of data. Additionally, both halos were mounted on the cadaver head by someone with no clinical experience. If this study were to be repeated, a clinician who would apply the halo to the patient and execute these tests could choose a slightly different position or orientation for the Bremer halo, thereby achieving more consistent results.

Neither the pins of the Bremer nor pins of the novel halo were tightened during Experiment 1. By tightening the pins of the novel halo, the moment arms become larger (with a maximum of 5 mm) as the distance between the halo and skull increases as the C-contour expands. The linear relationship between the axial pin force and the expansion of the C-contours for the novel halo is given in Appendix D.3.

By tightening the pins of the Bremer halo, the moment arms of the anterior pins were increased very little according to the high ring stiffness. The moment arms of the posterior pins increased by a maximum of 4,5 mm, which is demonstrated in Appendix A.1. In clinical practice the moment arms will therefore be larger than shown in this experiment as the halos expand during pin tightening.

This was the first attempt to create a customized halo ring according to CT input data. Therefore, the sample size (N) was 1. By increasing the sample size, the validity and reliability of the procedure will be better demonstrated.

In the results of Experiment 2, pins 2 and 4 (both located on the same side of the cadaver head) seemed to be more prone to deviate than pins 1 and 3. During the application of the novel halo to the cadaver head, the focus was placed on positioning the halo, as it would in a clinical setting. Pin 2 and 4 were checked less compared to 1 and 3. This could have caused slight crooked placement of the halo, resulting in a more accurate positioning of pins 1 and 3 than pins 2 and 4. The accuracy and precision of pins 2 and 4 were therefore shown to be lower than they could have been.

5.4 Conclusions

5.4.1 Experiment 1

By designing a customized halo, the moment arms turned out to be smaller and closer to each other than those of the Bremer halo. The differences of the novel halo in pin orientation were less than those of the Bremer halo.

Pin 1 of the Bremer halo showed a difference of 17° for the β -angle, which was expected to lead to decreased biomechanical pin characteristics[16].

5.4.2 Experiment 2

The procedure from acquiring the geometrical data of the cadaver head to fabricating the novel halo did not introduce any unexpected variances in sizes and shape. It is suggested that this procedure can be used to create customized halo rings.

Moment arms. The moment arms of the pins shown in Table 3 did not vary more than 3 mm during a single test. The modeled moment arm in 3D CAD software was representative of the moment arms in reality. Thus, the procedure for modeling the moment arms is suitable for the design of future novel halos.

Pin positions. The deviations from the intended positions were within an acceptable range, since the anterior pins were still placed in the validated safe region by K. Semmelink[29].

α and β . Both α and β were within an acceptable range and did not go beyond a difference of $>15^\circ$ and the novel halo would therefore be safe to use for HGT.

5.4.3 General

By customizing the halo, based on CT data, the pins can be positioned and orientated desired on the head of a patient (at a novel anterior pin location). All the deviations from the intended values in the novel halo would not cause any unsafe situations for the patient (cadaver head in this case).

6 Part II. Axial pin force control

The spring characteristics at each C-contour were custom designed and evaluated on the cadaver head to map the degradation of the axial force over time.

In addition, the behavior of the novel halo regarding pin reaction forces was analyzed. Mapping the responses of the pins to each other was intended to demonstrate that tightening a pin in the novel halo actually would result in the intended force on the opposing pin. When both C-contours were connected by the bridge connector, the influence of this connector was evaluated on the tightening and loosening of the pins. With this information suggestion was made to improve the design of the novel halo to decrease its bulkiness.

6.1 Visco-elasticity of the cadaver head

It appeared that the very high stiffness of the Bremer ring at the anterior pin location did not allow the retention of sufficient force on the anterior pins. A small displacement of the ring resulted in a high reduction of force generated by the pins. Displacement occurred due to the visco-elastic and creep nature of the bone. To avoid pin loosening, the stiffness of the ring at the pin site locations should allow the pin to load at a sufficient amount of axial pin force to prevent the pin from loosening over the entire 3-month traction period. No clinical trials were been performed with the novel halo but prediction was made, based on a 24 h trial on the cadaver head.

6.1.1 Methods

To measure the axial pin force, strain gauges were attached to the novel halo at 4 positions, corresponding to the positions of the highest stress state in the material during pin tightening. The details about the placement and calibration of these strain gauges can be found in Appendix F. By calibration, the strain gauges were able to relate a force at a certain position to a certain voltage difference. The difference in voltage was measured and recorded. At least 20 min before each test, the strain gauges were turned on to warm up, so that temperature differences would not influence the measurements. During each test, the strain gauges were manually stretched up to a voltage difference of 7 Volts (V). The positions of the strain gauges and their corresponding pins are shown in Figure 25.

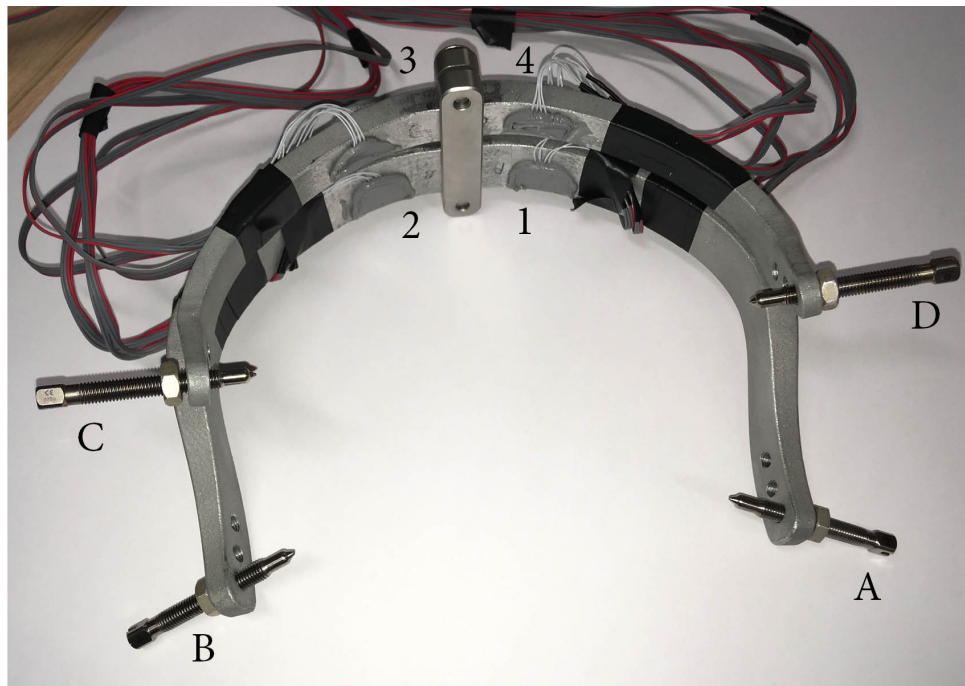


Figure 25: Four strain gauges (1, 2, 3 and 4) and their corresponding pins (A, B, C and D).

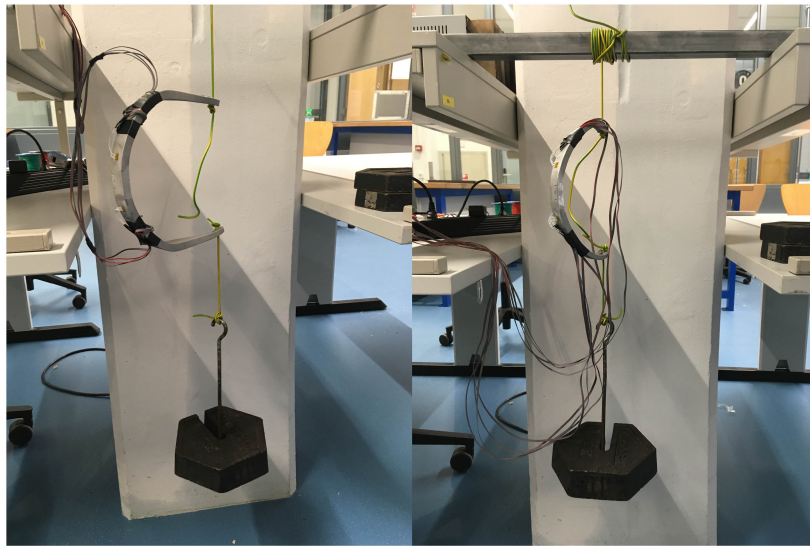
Twenty-four hours prior to each test, the cadaver head was defrosted to room temperature (approximately 25°C). The pins were tightened to a 7 volts difference and locked with a lock nut. Three tests were performed before filtering the visco-elasticity of the skull.

Hanging free. To obtain the information on the response of the strain gauges in a basic and predictable loading condition, the novel halo was hung while being able to move freely, as shown in Figure 26(a). A force of 343.35 N (i.e. 35 kg, black weights) was added to each of the C-contours. The strains in the material were measured for 24 h.

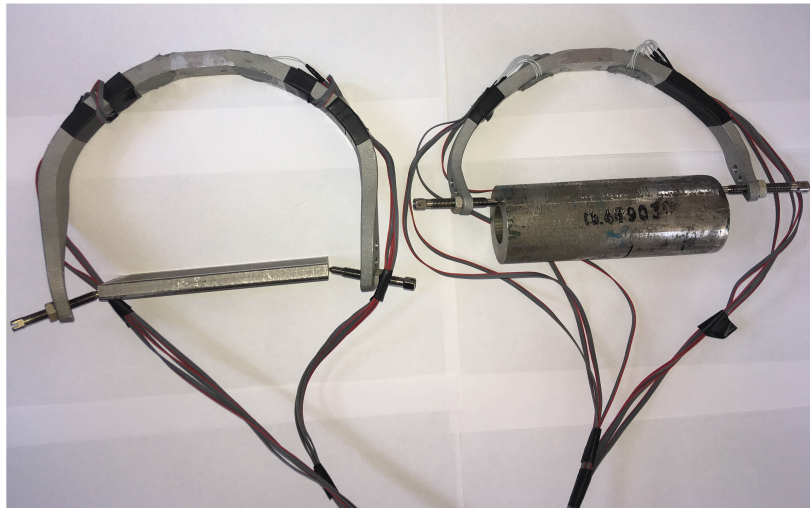
Steel. Both C-contours of the halo were mounted on a piece of stainless steel, as shown in Figure 26(b). The steel ensured that very little visco-elastic responses occurred. The data obtained was compared later on to the data obtained on a cadaver head from which the effect of visco-elasticity of the skull could be derived.

The pins were tightened to a voltage difference of 7 volts. The strains in the material were measured for 24 h.

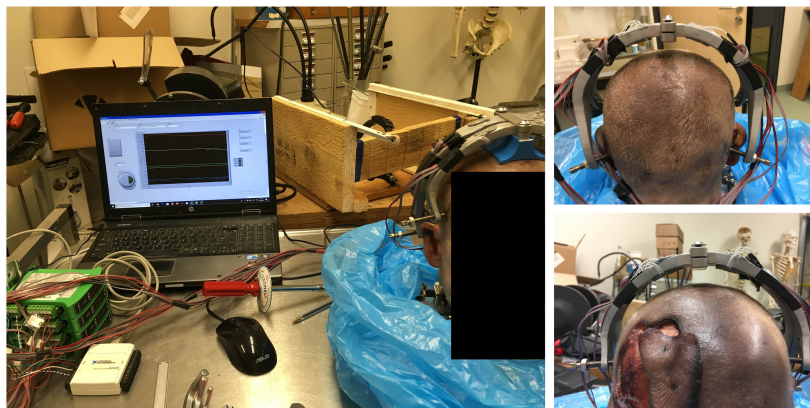
Cadaver. The halo was placed on the cranium of the cadaver head as shown in Figure 26(c). The strain in the material was measured for 24 h.



(a)



(b)



(c)

Figure 26: (a) 35 kg of weight is hung freely on both C-contours for 24 h. (b) 7 Volts difference applied to both C-contours and settled for 24 h. (c) 7 Volts difference applied to both C-contours and settled on a cadaver head for 24 h.

6.1.2 Results

Figure 27 shows the results of the three tests performed with the novel halo.

Hanging free. Figure 27(a) shows the situation where both C-contours were hung freely in air by a weight of 35 kg attached to one side for 24 h. In the graph, each strain gauge, represented by a letter, contains two lines. The dotted line represents the original data obtained from the strain gauge. This line shows the decrease in force over time, which were not expected. This was due to the effect of the creep of the glue used to attach the strain gauge to the C-contours[36]. The differences between the dotted line and solid line were used to correct the results of the other tests, since this creep effect would also be present during these tests.

Steel. The decreases from the initial force to the remaining forces after 24 h were -4,4%, -11,6%, -8,46% and -10.91% at A, B, C and D respectively. During the first 500 s, the drops in force were relatively larger, than those during the remaining seconds. According to the '*Handbook of Bolts and Bolted Joints*', surfaces of new bolts and joints always have peaks and valleys[37]. Plastic deformation is a result of very high stresses at the small surfaces of these peaks. Deformation at the thread interface means that the ring is able to move slightly relative to the pin and will result in a reduction in strain. These effects are microscopic and therefore will not be the only reason for the reduction. Abid et al., (2015) considered multiple reasons for short-term relaxation within the first seconds or minutes after tightening: *"Most of the relaxation occurs shortly, after the joint has been assembled or at least soon after it has been put into service, due to a number of reasons, such as bolt bending, soft parts (gasket), improper tooling and torqueing, bolt quality, non-parallelism of flange joint surfaces, geometric variance and so on"* [38].

The remaining part of the graph showed a trend, characteristic of the graph that one would find during stress relaxation tests. Because the effects of the creep of the glue to the strain gauges and stress relaxation in the C-contours had been compensated in this graph, there must be another effect dominating the trend of this curve. Since the only left over variables were the pins and the steel to which the pins were mounted, these must have caused the slight drop in force over time. According to the findings of Liu et al., (2001) even high strength steels are subjected to the phenomena creep and stress relaxation at stress levels corresponding to $1/3\sigma_{0.2}$ [14]. These stress levels were reached during this test, which was confirmed by FEM.

Cadaver. During the test on the cadaver head, a similar trend to that observed during the test on steel was found. Also the initial drop in force occurred at the beginning, which could be assumed to be the initial settling of the thread and all other reasons described by Abid et al., (2015). However, the reductions in force were larger than the reductions found in steel which were -3,2%, -6.8%, -5,2% and -5,6% at A, B, C and D at $t = 500$ s respectively. According to the observation of Sasaki & Enyo (1995), the visco-elastic nature of the bone has a tendency to reduce stress over time. An equilibrium is reached when the graphs reach a theoretical asymptote of their function at $t = 7,776,000$ s (which corresponds to 3 months). This leads to a reduction in force to 365, 317, 280 and 246 N for pins A, B, C and D respectively.

Figure 27(d) presents the isolated effect of the visco-elasticity of the skull of the cadaver head on the strain gauges. Strain gauges 1 and 2 showed the same percentage decrease. However, strain gauges 3 and 4 showed a slightly different decrease from each other. If the density and visco-elastic behavior of the skull are not completely homogeneous, any deviations in one of these characteristics would result in the differences in strain at the strain gauges and thus differences in force. The reduction in force solely due to the visco-elastic behavior of the cadaver skull would be on average 19 N at each pin site after one day, which was 3% of its initial axial pin force. This would lead to a reduction of 0.34 mm in displacement at the anterior C-contour and 0.43 mm at the posterior C-contour according to their stiffness values.

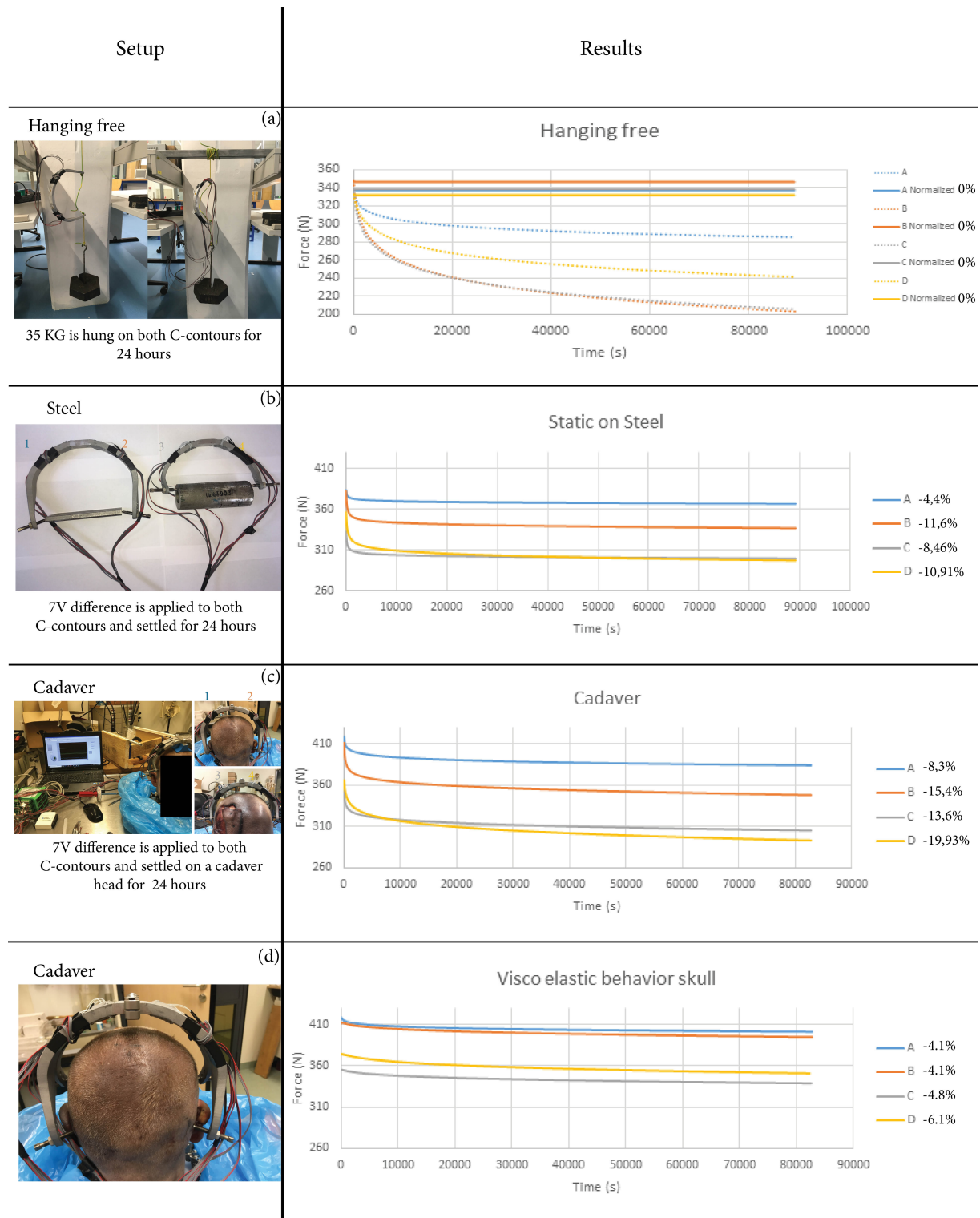


Figure 27: (a) 35 kg is hung on both C-contours to be used as a reference measurement. (b) both C-contours are mounted on steel. Compared to (a), the mechanical behavior of the steel and the thread caused a decrease in strain, mainly during the first 500 s. (c) Novel halo mounted on the cadaver head. (d) The isolated effect of the visco-elastic behavior of the skull on the axial pin force.

6.1.3 Discussion

Cadaver head. All the tests were performed on the cadaver head but not on living patients. In other words, the performance of the novel halo on living bone tissue was not evaluated. Since the physiological processes occurring in living bone are more dynamic, it is predicted that an increased force reduction over time may occur.

Strain gauges. Strain gauge 1 was less susceptible to the reduction in force, compared to the other strain gauges. During the placement of the strain gauge, a different type of glue was used for strain gauge 1 from that for the other strain gauges.

The observed decrease in force in the 'hanging free' situation was due to the creep effect of the glue. It was assumed that this effect would be the same during each test, just as the effects of creep and hysteresis in the base material (AlSi10Mg) and could therefore be used for the compensation of the other tests for extracting the visco-elastic behavior of the skull. However, if any of these effects was not completely the same, the results would be influenced. No tests were performed to validate the repeatability of each test. Therefore, the results should be interpreted with caution. Especially concerning the extracted visco-elastic behavior of the skull, as the reductions found are very small.

No traction force. No traction force was applied during any of these tests. In clinical practice, however, a traction force is present, which will cause shear forces at the pin/skull interface leading to increased force reductions over time as the bone will deform more.

6.1.4 Conclusion

Based on the extrapolation of the data of the cadaver head to a period of 3 months, prediction was made that both C-contours with their own stiffness values would be able to maintain their forces to a point where an axial force of 200 N could still be applied without the need of re-tightening.

6.2 Pin reaction forces

The novel halo had two separate C-contours. Theoretically, each pin force would therefore be the result of the force applied to the opposing pin. However, during the design phase, there were two design considerations for the bridge that connected the two C-contours. The first design used the bridge to only clamp the two C-contours, but the question remained regarding the functioning of this concept. The second design used a bridge integrated into both contours, instead of being a separate part. The influence of connecting both C-contours, before tightening, on the accuracy of achieving an intended axial pin force remained unclear.

Almost all pins in the Bremer halo affect each other. When one pin was tightened, other pins popped out of place as demonstrated in Section 2.2.2: *Undefined pin reaction forces*. This section also analyzes the behavior of the novel halo regarding the pin reaction forces. By mapping the responses of the pins to each other, it was intended to demonstrate that tightening the pins in the novel halo actually will result in the intended force at the opposing pin. Therefore, this section aimed to resolve the following points:

- Determine the influence of connecting the bridge on the accuracy of pin tightening
- Define the improvements during pin tightening in axial pin responses, compared to the Bremer halo

6.2.1 Methods

Determine the influence of connecting the bridge before pin tightening. First, both the pins of the anterior and posterior C-contour were tightened to steel without the bridge connecting these two C-contours (Figure 52 (a)). After tightening the pins in the order of A and B, then C and D (the same for both tests), the bridge was connected to both C-contours. This procedure was compared to the tightening procedure for the Bremer halo.

Second, both the anterior C-contour and posterior C-contour were connected by the bridge prior to pin tightening (Figure 52 (b)). The pins of the anterior C-contour were tightened on a steel surface after the pins of the posterior C-contour were tightened onto a steel surface.

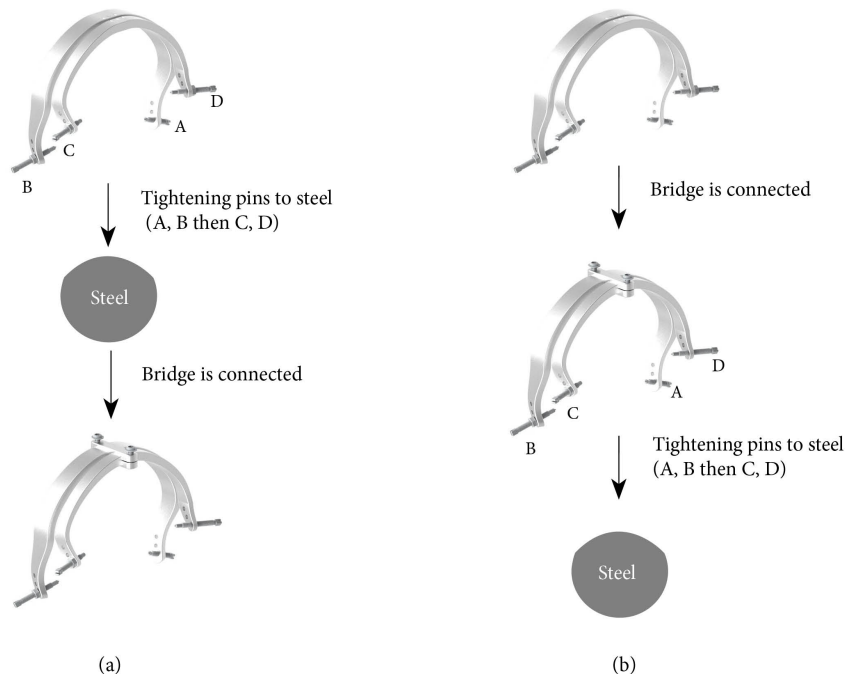


Figure 28: (a) First tighten the pins of both C-contours after the bridge is attached. (b) The bridge is connected before tightening the pins.

6.2.2 Results

Determine the influence of connecting the bridge before pin tightening. The results from investigating situation (a) demonstrated that during tightening none of the pins influenced each other, since both C-contours were not connected. When the bridge was locked, a shift in axial pin force occurred. This shift was caused by the surface of the C-contours being not completely flat and resulted in a deviation of $\pm 10\%$ in axial pin force from the intended axial pin force. The surface of the bridge therefore forced the C-contour to move in a certain direction, causing the (contra) reactions in force at both C-contours. This effect will be further discussed in Section 6.2.3.

In situation (b), the responses of pins A and B to the tightening of pin D occurred from $F_D = 50N$ (F_D is the axial force of pin D) until $F_D = 175N$. Pin A showed a slight decrease in axial pin force, while pin B showed a slight increase in axial pin force. Also here, this contra reaction in axial pin force between pins A and B was believed to be caused by a slight misalignment of the C-contours with respect to each other and by the non-symmetrical tightening of pins C and D. At $F_D = 175N$, pin C was tightened and the responses of in axial pin force of pins A and B were converted compared to their responses given at $F_D = 50N$. After finishing tightening (at $t = 250s$), a deviation in force between pins A and B remained visible of $\pm 4\%$ from the intended value. During clinical application of the novel halo it is not expected that perfect alignment will be possible, or perfect symmetric tightening. Therefore, this deviation in force cannot be avoided.

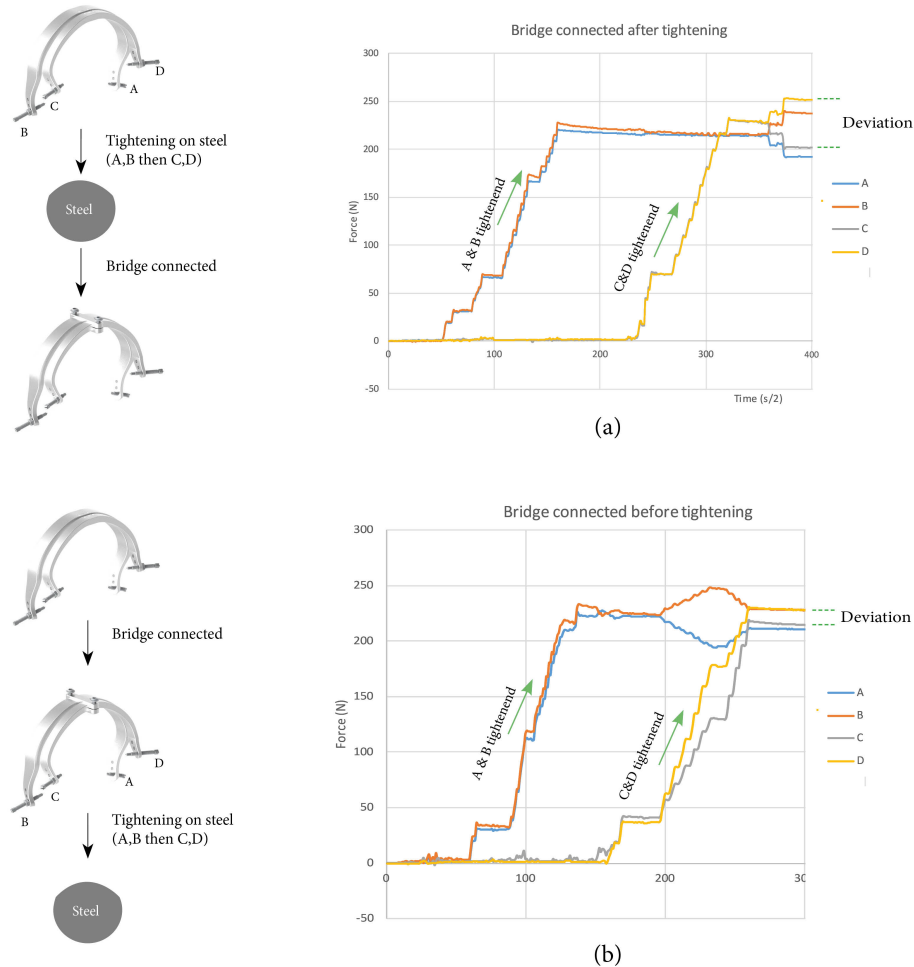


Figure 29: (a) Effect of tightening on the axial pin forces when the bridge is not connected. (b) influence of the bridge connected before tightening on the axial pin forces.

Improvements compared to the Bremer halo. It was demonstrated that the tightening of any of the pins in the Bremer halo resulted in axial and non-axial forces on the other pins. Some pins even popped out of their conical hole, indicating high non-axial pin forces. The domination by other resulting forces than the axial pin force, gave insight in the unpredictable and over-defined nature of the Bremer halo.

Consider the situation given in Figure 29(b). Tightening a pin of one C-contour only influenced its opposing pin. The over-defined response due to the tightening of the second C-contour produced predictable axial pin forces. Eventually after the pins are tightened, the accuracy of the pin forces will be dependent on the error during measuring the displacement of the ends of a C-contour (human and caliper error) combined with an error of 4% and 1.5% (which was the error of the strain gauges, see Section 7).

6.2.3 Discussion

The surfaces between the bridge and both C-contours are apparently not parallel or perfectly aligned, causing an undesired enforced movement of the contours during tightening of the bridge, as illustrated in Figure 30. The bridge was fabricated by using a milling machine and was perfectly flat. The non-parallelism was present in the C-contours and was caused by the restrictions of the selective laser sintering process at Oceanz. This non-parallelism, together with some non-symmetric tightening of the pins, caused a difference in pin force.

If perfect alignment and tightening would be assumed between the bridge and contours, theoretically, no offset in force would occur when tightening the bridge. Now there was an offset of $\pm 10\%$ present.

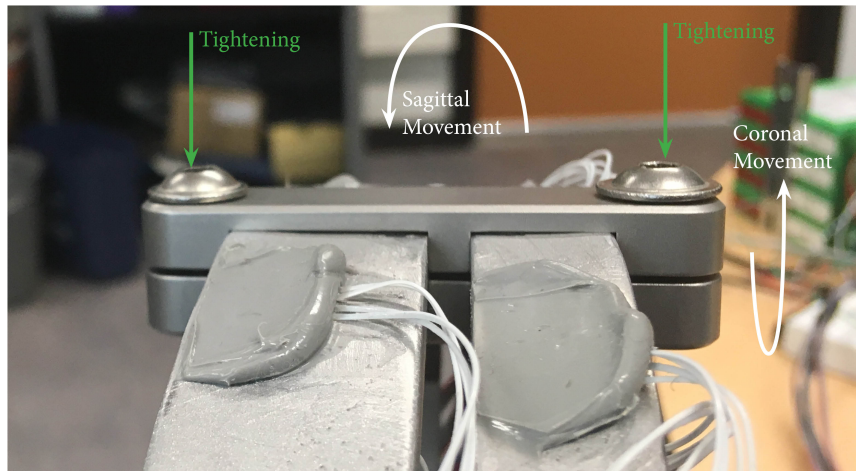


Figure 30: Tightening the bolts of the bridge caused both C-contours to move in the two directions (in the coronal and the sagittal plane), affecting the strains at the strain gauge sites.

6.2.4 Conclusion

Determine the influence of connecting the bridge before pin tightening. Connecting the bridge before pin tightening affected the tightening characteristics of the halo. However, the highest accuracy in the axial pin force was achieved when the bridge was connected before pin tightening, which facilitates the clinician in assessing the axial pin force. Therefore, the bridge could be incorporated into C-contours in future designs, which would make the halo less bulky. An example of such integration is given in Figure 31.

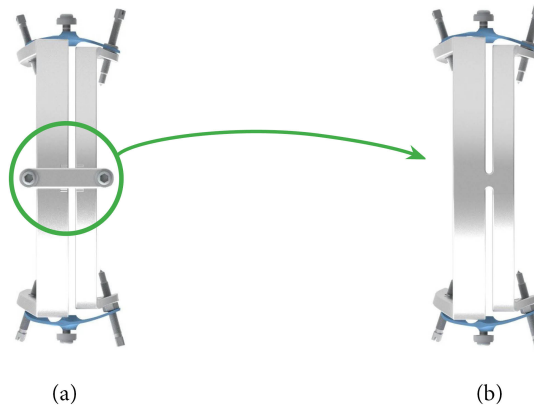


Figure 31: (a) Novel halo with the bridge. (b) proposal for an alternative solution when the bridge is incorporated into both C-contours

Improvements compared to the Bremer halo. The over-defined system of the novel halo, which was created after the tightening of pins of one C-contour, was more predictable in the axial pin force than the over-defined system in the Bremer halo. A clinician is now able to approximate the amount of axial force applied to a pin with an accuracy of 94,5% (human error not included).

7 General discussion

Novel pin position. The anterior pin position was new and never used in practice. A clinical trial should point out whether the new location indeed induces any unforeseen uncomfortable situations for the patient.

Pin positioning. When determining a safe position for placing a pin, a circumferential region should be assigned to visualize the potential spread from the intended position. A clinician should always visually check what the exact positions of the pins on the skull will become before tightening. Additionally, they should be aware that variances between the model and reality may be introduced during the procedure of customizing the halo.

Cadaver head. In this study, all the tests conducted were performed on a male cadaver head of approximately 65 years of age. More representative results could have been achieved if these tests were conducted on a child's cadaver head.

Axial pin force. In the novel halo, a maximum axial pin force of 450 N was used. This value was derived from the torque values found in the literature. However, there is a paradox about the relationship between the load applied to pins and pin loosening, since a higher load may induce bone necrosis and bone remodeling and thus pin loosening[33]. Clinical trials should be performed to point out the exact degradation in force over time with an initial pin force of 450 N. If the degradation is too high (pins tend to loosen), the initial pin-force should be reconsidered and the stiffness of the C-contours should be reduced accordingly. This would result in decreases in the dimensions of the C-contours and facilitates a slimmer design.

When reconsidering the stiffness of C-contours, one should be aware that the C-contours do not become too limp so that their performance would be affected when external and dynamic forces are applied. For example, when the patient bumps or makes extensive movements.

Strain gauges. The strain gauges have measurement errors in their output, which were not taken into consideration in this study. The technical datasheet obtained from HBM is displayed in Appendix F.4. In this data sheet the gauge factor (K) of $1.96 \pm 1.5\%$ is shown. This gauge factor is a constant, relating the change in resistance to the change in the length of a wire. The deviation in this factor is a measure of the accuracy of the measurements when the strain gauges were used.

Procedure. Before any procedures for the customization of halos are standardized, they should be validated. A notifiable difference was found between the assigned stiffness of the anterior C-contour in the CAD model, and the stiffness found in reality. In this research, the procedures from CT scan to testing in reality was performed only once. The procedures followed in this study should be considered as exploratory research. It is advised to examine the procedures on their validity in the follow-up research.

8 General conclusion

Table 5 summarizes the shortcomings of the Bremer halo in comparison with the novel halo to demonstrate the improvements achieved.

Shortcomings	Improvements
Generalized in size	Customized
Visible scars	No visible scars
High anterior ring stiffness	Customized stiffness
Undefined pin reaction forces	Defined pin reaction forces
Torque-based tightening	Displacement-based tightening

Table 5: Shortcomings of the Bremer halo and the improvements of the novel halo.

I. Customization

The goal of the present study was to design, produce and test a customized halo to control the moment arms, pin positions and pin orientations in order to address the issues of the Bremer halo with respect to pin loosening and bulkiness.

- Customized halo.

By customizing the halo, the parameters, such as the moment arm, pin-orientation and pin-position, can be controlled and used as input parameters for creating a 3D model of both C-contours. The novel halo indeed has smaller and more consistent moment arms compared to those of the Bremer halo. The deviations resulting from going through the procedures from CT scan to 3D printed halo rings are acceptable. However, the clinician should be aware of the potential spread that may occur during the placement of the halo, especially for the patients with decreased skull properties or cranioplasty (a surgical procedure, where a part of the skull is revised and replaced).

- Novel anterior pin locations.

Because the anterior pin position of the novel halo is placed at the hairline in the musculus temporalis region, there will be no visible scars after the HGT treatment, assuming that the patient has hair.

II. Axial pin force control

The goal of controlling the axial pin force was to reduce pin loosening by introducing a customized ring stiffness.

- Customized ring stiffness.

Pin force degradation over time was dependent on the stiffness of the C-contour.

The stiffness of the novel ring at the anterior pins was predicted to be sufficient to maintain sufficient axial pin forces during a traction period of 3 months. The Bremer halo was clinically proven to show pin loosening during this same period.

Clinical trials should eventually clarify what tightening procedure should be followed over a 3 month traction period.

- Well-defined pin reaction forces during tightening.

Tightening a pin in the novel halo only effected its opposing pin, while tightening a pin in a Bremer halo effected almost all the other pins and also induced forces which made pins pop out of place.

- Displacement-based pin tightening.

Due to the dependency on thread friction (combined with non-axial pin forces), tool-accuracy (61%) and even variances between clinicians make pin tightening, applied by torque, a highly inaccurate procedure.

In the novel halo pin tightening was controlled by the displacement of the C-contour. The accuracy of the axial pin forces would be dependent upon the caliper error combined with an axial pin force deviation of $\pm 4\%$. The clinician is now able to get an indication of the axial pin forces by measuring the difference in distance between the ends of both C-contours and by multiplying this difference by $55 \frac{N}{mm}$ or $44 \frac{N}{mm}$.

9 Recommendations

(1) Perform an oscillatory experiment. By doing so, the daily life activities of the patient will be mimicked. The halo should be connected to the same cadaver head and the anterior and posterior C-contours should be tightened to displacements of 7 and 9 mm respectively (this would correspond to roughly 400 N). Normally, the head moves up and down at an amplitude of 1,25 cm and a frequency of 1.4 Hz[39][40]. By moving the cadaver head at this frequency and amplitude for a day, the halo can be assessed on its functioning under dynamic conditions. This dynamic test will expose the halo not only to standard traction forces, but also to impact forces, when the head moves up and down (and perhaps even sideways). Even though the patient in UMC Utrecht is not always able to walk, records can be found in which patients can walk. Also, some patients in the wheelchair are still very movable with their posture and head during the HGT treatment. An example of a setup to evaluate the novel halo in this situation is presented in Figure 32.

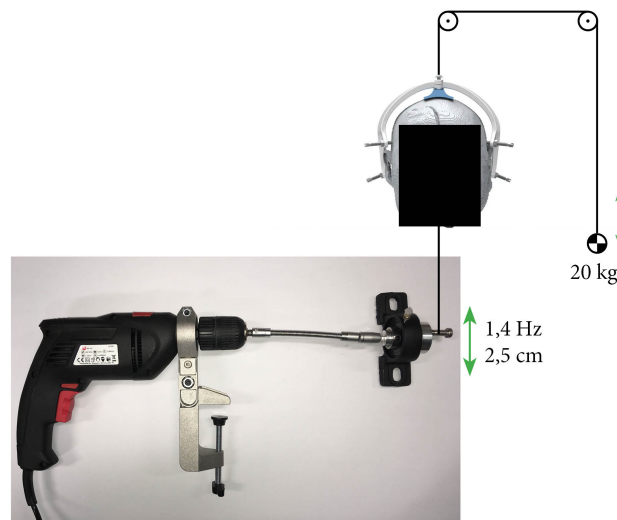


Figure 32: An example of a test setup that may be used to induce movements to evaluate the influence of dynamic effects on the novel halo.

(2) Subject the novel halo to MRI. Some patients are assessed on the efficacy of HGT (during the treatment) using MRI. The Bremer halo contains a plastic part on top of the ring. This is to prevent the aluminum loop from closing. When the halo is subjected to MRI, a closed aluminum loop may induce heat which will make the patient feel uncomfortable. The novel halo was not designed and constructed to have such a loop. However, to ensure that no heating will occur during MRI, the halo should be exposed to MRI in the same magnetic field. The temperatures of the C-contours will be measured to be sure if they are within an acceptable limit.

(3) Re-evaluate the connection for the traction rim before clinical use. The connection is now constructed by means of Fused Filament Fabrication (more commonly known as 3D printing) using Acrylonitrile Butadiene Styrene (ABS). This fabrication method has the disadvantage that the interface between two layers is relatively weak, which may cause delamination and thus the failure of the part.

Even though the connection was proven to be able to hold 36 kg of traction (see Appendix G), it is recommended to test this part thoroughly in order to be sure that it will not fail during the 3-month period of traction or use a different fabrication method where delamination is not an issue anymore.

While ABS has been used for its relatively high stiffness, alternative materials may be investigated and used for this part. Additionally, plastics can be manufactured in a large variety of colors, which offers the opportunity for the patients to choose the color for the connection rim, if that is feasible.

(4) Explore alternatives to determine the input data for the customized halo ring. Currently, 3D scanners are available, which may be used in stead of CT. Prior to 3D scanning, the clinician places markers on the head of the patient. These markers may be used as coordinates for the 3D model to generate a customized halo. The other parameters such as the moment arm and pin orientation are prescribed in Solid Edge ST 10 and will be used to generate a model of a novel halo ring, having the characteristics of the ring, as described in this research. In a most ideal scenario, the pin positions are obtained from 3D scanning the patient. These parameters are then translated into X-, Y- and Z-coordinates which are used as input parameters. A pre-programmed parameterized algorithm in Solid Edge ST 10 would then create the geometry of the c-contours.

(5) Do not use strain gauges for multiple load situations. Strain gauges are a good tool to measure elongation and to relate elongation to a given force in a given direction. However, by introducing different forces (such as the traction force) from the calibrated forces, it is hard to distinguish the effects of any of these forces measured by the strain gauges.

(6) Decrease the bulkiness. This wish will be achieved by decreasing the dimensions of both C-contours. This is achieved by:

- Connecting both C-contours. The bridge can be incorporated into future designs, which would make the halo less bulky.
- Differentiating the material. If a stiffer material is used (e.g., the titanium alloy Ti-6Al-4V, medical grade) the dimensions of the C-contours can be reduced. Oceanz is able to selectively laser sinter this material. This material has a Young's modulus of 110 GPa, which is roughly twice as stiff as the AlSi10Mg alloy. This means that the thickness of the ring can be reduced to 8 mm instead of 11 mm (according to FEM analysis), while the C-contour retains the same displacement at the pins. Bear in mind however, that selective laser sintering of Ti-6Al-4V alloy will increase production costs.
- Reducing stiffness, if the stiffness of the C-contours can be reduced, the dimensions of the contours can be reduced accordingly.

(7) Reduce costs. The total costs of producing the novel halo were around EUR 1,400 while the current halo systems are purchased at a price of EUR 1,100. Even though the novel halo was used for the research project and thus the focus was not placed on creating a cost efficient product, financial consideration should always be given for future commercialization. The majority of the costs were related to producing both C-contours by means of SLS by Oceanz. The geometry of both contours was not complex. Therefore, an alternative fabrication method may be used to reduce the costs.

(8) The complexity of the procedures will be reduced when the steps in the customization process are automated. The parameters, such as pin position and pin orientation, were parameterized. Theoretically, one can fill in these parameters, resulting in a new customized geometry of a halo. The settings for determining the stiffness of the C-contour was done manually, but were estimated by an optimization algorithm in Solid Edge ST 10. Customizing halos will be feasible, if the necessary design steps are minimized and less complex.

10 References

- [1] Zuccarello Nick. Planes of human anatomy; 2008. Available from: https://commons.wikimedia.org/wiki/File:Human_anatomy_planes.svg.
- [2] Watanabe K, Lenke LG, Bridwell KH, Kim YJ, Hensley M, Koester L. Efficacy of perioperative halo-gravity traction for treatment of severe scoliosis (100). *Journal of Orthopaedic Science*. 2010;15(6):720–730.
- [3] Lawhon S, Crawford A. Traction in the treatment of spinal deformity; 1983.
- [4] Garabekyan T, Hosseinzadeh P, Iwinski HJ, Muchow RD, Talwalkar VR, Walker J, et al. The results of preoperative halo-gravity traction in children with severe spinal deformity. *Journal of Pediatric Orthopaedics B*. 2014;23(1):1–5.
- [5] Rinella A1, Lenke L, Whitaker C, Kim Y, Park SS, Peelle M, Edwards C 2nd BK. Perioperative halo-gravity traction in the treatment of severe scoliosis and kyphosis.; 2005.
- [6] Koller H, Zenner J, Gajic V, Meier O, Ferraris L, Hitz W. The impact of halo-gravity traction on curve rigidity and pulmonary function in the treatment of severe and rigid scoliosis and kyphoscoliosis: a clinical study and narrative review of the literature; 2012.
- [7] Mehrpour S, Sorbi R, Rezaei R, Mazda K. Posterior-only surgery with preoperative skeletal traction for management of severe scoliosis.; 2017.
- [8] Nemeth JA, Mattingly LG. Six-pin halo fixation and the resulting prevalence of pin-site complications. *The Journal of bone and joint surgery American volume*. 2001;83-A(3):377–382.
- [9] Garfin SR, Botte MJ, Waters RL, Nickel VL. Complications in the use of the halo fixation device.; 1986.
- [10] Saeed MU, Dacuyucy MAC, Kennedy DJ. Halo pin insertion-associated brain abscess: case report and review of literature. *Spine*. 2007;32(8):E271–4.
- [11] Lerman JA, Haynes RJ. Open versus closed halo rings: comparison of fixation strengths. *Spine*. 2001;26(19):2102–2104.
- [12] Glenn P, Kerwin A, Kelving L, Drake B, White MD, Kun-Ling S, Saliccioli GG, King H, et al . Investigation of how different halos influence pin forces; 1994.
- [13] Smith MD, Johnson LJ, Perra JH, Rawlins BA. A biomechanical study of torque and accuracy of halo pin insertional devices. *Journal of Bone and Joint Surgery - Series A*. 1996;78(2):231–238.
- [14] Stephen HL, Lunsford R, Waters RL . The Effect of Local Halo Pin Care Reagents on Cranial Radial Compressive Stress (When Tightening Halo Pins). *Journal of Prosthetics and Orthotics*. 1993;5(3).
- [15] Klingenberg J, Keown A, Moser D, Neal T, Stamper R. A new method of tightening halo orthosis pins that reduces initial pin force variation.; 2002.
- [16] Triggs KJ, Ballock RT, Lee TQ, Woo SL, Garfin SR. The effect of angled insertion on halo pin fixation.; 1989.
- [17] Children Schwend MK City. Pull Off Strength of 6 and 10 Pin Halo Fixation in Sawbones Skulls Pull Off Strength of 6 and 10 Pin Halo Fixation in Sawbones Skulls; 2016.
- [18] Ballock RT, Lee TQ, Triggs KJ, Woo SL, Garfin SR. The effect of pin location on the rigidity of the halo pin-bone interface.; 1990.
- [19] Ebraheim NA, Lu J, Biyani A, Brown JA. Anatomic considerations of halo pin placement.; 1996.
- [20] Papagelopoulos PJ, Sapkas GS, Kateros KT, Papadakis SA, Vlamis JA, Falagas ME. Halo pin intracranial penetration and epidural abscess in a patient with a previous cranioplasty: case report and review of the literature. *Spine*. 2001;26(19):E463–E467.
- [21] Manuscript A. Gender and Elastic Modulus. 2013;30(5):693–699.

- [22] Bembey AK, Oyen ML, Bushby AJ, Boyde A. Viscoelastic properties of bone as a function of hydration state determined by nanoindentation. *Philosophical Magazine*. 2006;86(33-35 SPEC. ISSUE):5691–5703.
- [23] Cammarata M, Nicoletti F, Di Paola M, Valenza A, Zummo G. Mechanical behavior of human bones with different saturation levels. *Proceedings of 2nd International Electronic Conference on Materials*. 2016;p. B003.
- [24] Davis MT, Loyd AM, Shen HyH, Mulroy MH, Nightingale RW, Myers BS, et al. The mechanical and morphological properties of 6 year-old cranial bone. *Journal of Biomechanics*. 2012;45(15):2493–2498.
- [25] McElhaney JH, Fogle JL, Melvin JW, Haynes RR, Roberts VL, Alem NM. Mechanical properties of cranial bone. *Journal of Biomechanics*. 1970;3(5):495–496,IN5,497–511.
- [26] Reilly DT, Burstein AH. The elastic and ultimate properties of compact bone tissue. *Journal of Biomechanics*. 1975;8(6).
- [27] Karnes J, Moench K, Ordway NR, Stamper R, Trammell T. Determination of minimum required halo pin force. *Journal of Spinal Disorders & Techniques*. 2006;19(4):281–285.
- [28] Stone JL, Gulabani A, Gorelick G, Vannemreddy SNK, Vannemreddy PSSV. Frontolateral pins for halo ring placement: reassessment of a common neurosurgical procedure with CT measurements of skull thickness. *Journal of Neurosurgery-Spine*. 2013;19(6):744–749.
- [29] Semmelink K, Hekman EEG, Swaan A, Kruijt MC. New halo pin positioning; requirements of axial tightening and bone strength of the temporal region; 2018.
- [30] Botte MJ, Byrne TP, Abrams RA, Garfin SR. Halo Skeletal Fixation: Techniques of Application and Prevention of Complications. *The Journal of the American Academy of Orthopaedic Surgeons*. 1996;4(1):44–53.
- [31] Fleming BC, Huston DR, Krag MH, Sugihara S. Pin force measurement in a halo-vest orthosis, in vivo. *Journal of Biomechanics*. 1998;31(7):647–651.
- [32] O'Donnell PW, Anavian J, Switzer Ja, Morgan Ra. The history of the halo skeletal fixator. *Spine*. 2009;34(16):1736–9.
- [33] Voor MJ, Anderson RC, Hart RT. Stress analysis of halo pin insertion by non-linear finite element modeling. *Journal of Biomechanics*. 1997;30(9):903–909.
- [34] Whitesides TE, Mehserle WL, Hutton WC. The force exerted by the halo pin. A study comparing different halo systems; 1992.
- [35] Bullock S, Runciman JR. Biomechanical evaluation of two halo pin designs, with, and without, intact periosteum. *Journal of Biomechanics*. 2001;34(1):129–133.
- [36] Potma T. Rekstrookjes Meettechniek. N.V.Uitgeversmaatschappij Centrex Eindhoven;.
- [37] Bickford J. An Introduction to the Design and Behavior of Bolted Joints, Third edition; 1959.
- [38] Nijgh MP. Loss of pre-load in pre-tensioned bolts; 2016.
- [39] Cappozzo A. Analysis of the linear displacement of the head and trunk during walking at different speeds. *Journal of Biomechanics*. 1981;14(6):411–425.
- [40] Hirasaki E, Moore ST, Raphan T, Cohen B. Effects of walking velocity on vertical head and body movements during locomotion. *Experimental brain research*. 1999;127(2):117–130.
- [41] Bogunovic L, Lenke LG, Bridwell KH, Luhmann SJ. Preoperative halo-gravity traction for severe pediatric spinal deformity: Complications, radiographic correction and changes in pulmonary function. *Spine Deformity*. 2013;1(1):33–39.
- [42] Sponseller PD, Takenaga RK, Newton P, Boachie O, Flynn J, Letko L, et al. The use of traction in the treatment of severe spinal deformity. *Spine*. 2008;33(21):2305–2309.

11 Appendix

A Analysis of the Stiffness of the Bremer Halo

A.1 Displacement at posterior pin sites - Experimental measurement

A force gauge with a maximum capacity of 1000 N was attached to one of the posterior pin sites of the Bremer Halo. The setup is shown in Figure 33. A digital dial indicator with an accuracy of 0.01 mm was used to measure the displacement between the ends of the C-contour of the Bremer halo. Starting at a load of 30 N with increments of 30 N, the displacements were registered. The results are given in Figure 34.

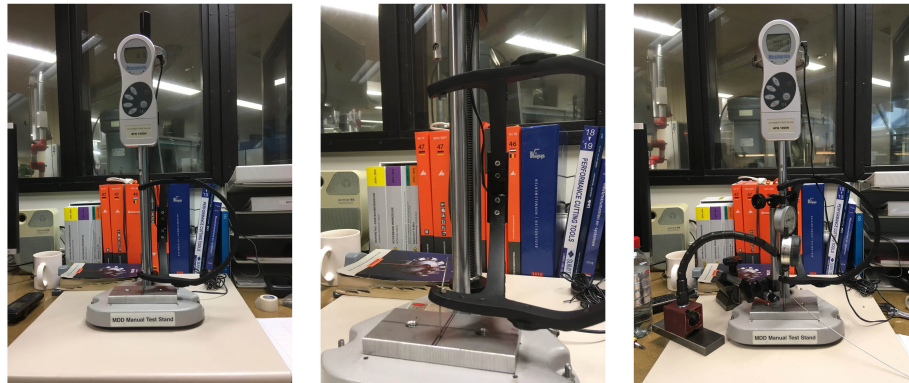


Figure 33: Overview of the test setup for measuring the stiffness of the C-contour of the Bremer halo at the posterior pin sites.

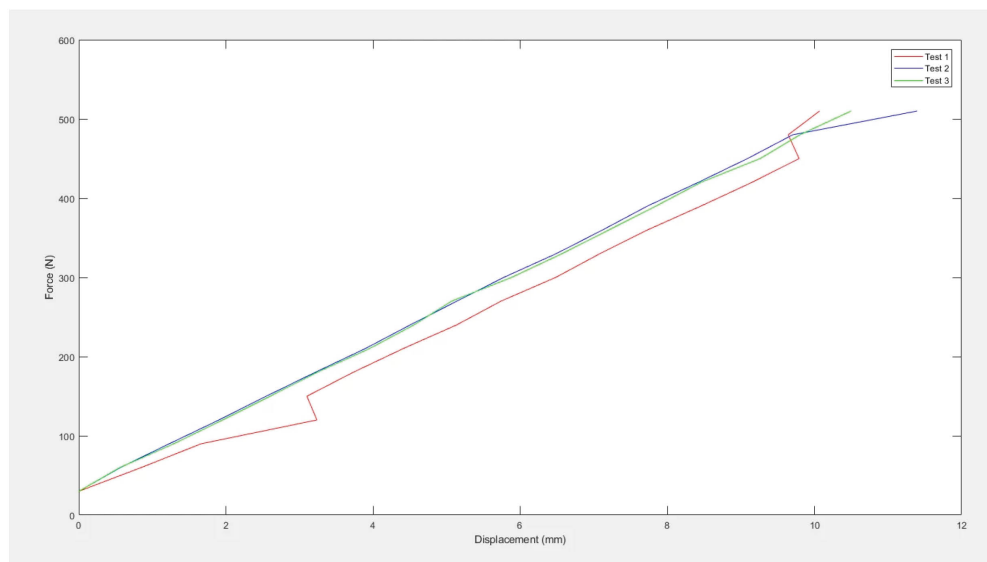


Figure 34: Displacements of the C-contour under different loads. The slope of all the lines is $50 \frac{\text{N}}{\text{mm}}$.

A.2 Displacement at posterior pin sites - FEM

A FEM analysis of the CAD modeled Bremer Halo was conducted to obtain indications of the displacement of the C-contour at the posterior pin site at given loads. The FEM model was validated by applying the same loading conditions, as described in Appendix A.1. The material of the Bremer halo ring was a casted aluminum alloy, assumed to be AlSi10Mg. The properties of this material were retrieved from the 3D metal printing company 'Oceanz' and are listed in Figure 35. No chemical analysis was conducted on the Bremer halo to retrieve its exact material composition.

Figure 36a illustrates the situation where the halo ring was subjected to FEM analysis. Starting at a load of 30 N, with increments of 30 N until a maximum of 510 N, the model is analyzed (which, not surprisingly, showed a linear relationship). Figure 36b shows the displacement at a load of 450 N. Note that half of the Bremer halo was subjected to FEM analysis. Considering the symmetry of the halo in the x-z plane illustrated in Figure 36a. The displacement shown in Figure 36b should be multiplied by 2 in order to obtain the total displacement between the posterior pin sites which has been measured in reality.

Comparison in displacement between the values given in Appendix A.1 and the slopes of the lines in

Figure 37 indicated that the FEM modeled Bremer halo ring had a higher stiffness. The C-contour predicted by FEM had a stiffness 1.3 times higher than the measured value. Several factors may have caused the discrepancy in the spring characteristics of the C-contours such as a difference between the CAD model geometry and real geometry, different material properties, a slightly different measurement position and the fact that FEM still is a numerical approach to reality with many assumptions and approximations. Considering these factors, the results from the FEM analysis could be interpreted and corrected by a factor of 1.3 in order to be able to use the model for further analysis.

FIT ALUMINUM		AlSi10Mg	
Material properties ¹⁾ Materialeigenschaften ¹⁾	Value as built wie gebaut	Value heat treated wärmebehandelt T6	Unit Einheit
Max. tensile strength Max. Zugfestigkeit	397±11	325±20	MPa
Modulus of elasticity E-Modul	64±10	65±5	GPa
Yield strength (R _{0.2}) Dehngrenze (R _p 0.2%)	227±11	220±20	MPa
Elongation at break Bruchdehnung	6±1	9±2	%
Reduction of area Brucheinschnürung	8±1	-	%
Hardness by Vickers Härte nach Vickers	117±1	-	HV10
Process-related properties Herstellungsspezifische Eigenschaften	Value as built wie gebaut	Value heat treated wärmebehandelt T6	Unit Einheit
Roughness (R _a /R _z) Rauheit (R _a /R _z)	4-6 / 25-35		µm
Achievable part accuracy Genauigkeit	± 100 ²⁾ / ± 0.2% of nom. ³⁾		µm

Figure 35: Data sheet of the aluminum alloy AlSi10Mg provided by the 3D metal printing company Oceanz.



Figure 36: (a) Half of the halo was subjected to FEM analysis fixed on all 6 degrees of freedom in the plane of symmetry. The applied force was parallel to the 'y-axis' which was the same direction as the force applied in the experiments, as shown in Figure 33. (b) Displacements at a load of 450 N is applied. The maximum displacement was used in this analysis.

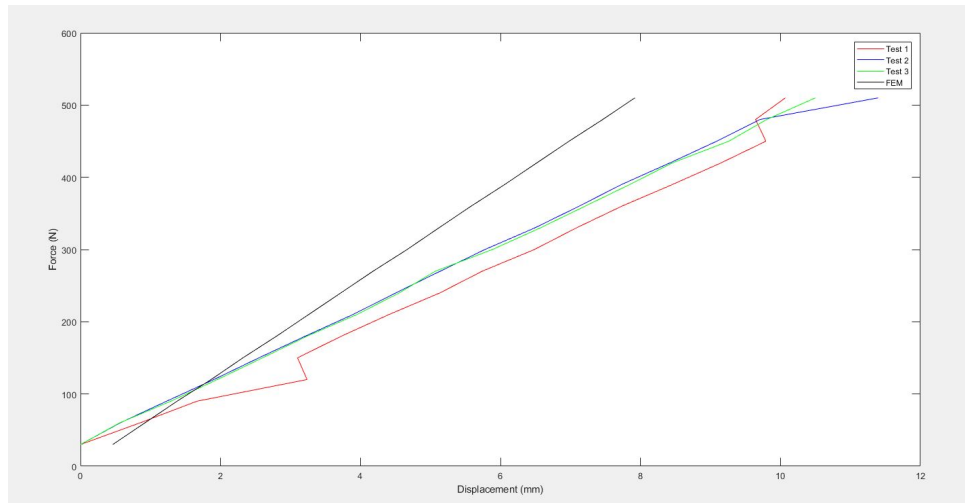


Figure 37: Black line represents the result of FEM. The red, blue and green line are the results of the experiment where the spring characteristic of a Bremer Halo at the pin positions is obtained. The result of FEM shows a spring characteristic (slope) of $65 \frac{N}{mm}$. The red, blue and green line have a slope of $50 \frac{N}{mm}$.

A.3 Displacement at anterior pin sites - FEM

FEM analysis of the CAD modeled Bremer halo was conducted to obtain indications on the displacement at the anterior pin sites at given loads. The same simulation conditions were applied as those described in Appendix A.2, except for the applied load. A load of 450 N was applied to the Bremer halo C-contour at the anterior pin site. Figure 38 shows the situation and the results obtained from the FEM analysis. A displacement of 0.16 mm was found at the anterior pin site.



Figure 38: (a) Half of the halo is subjected for analysis and fixed on all 6 degrees of freedom on the plane of symmetry. The applied force is in longitudinal direction of the anterior pin. (b) Results of situation when 450 N is applied. The maximum displacement at this location is 0.16 mm

Interpretation of this data should be done by realizing that in the situation above, the displacement only occurred due to the displacement of the ring. In a clinical situation, the displacement will probably be higher, because the remaining pins are not infinitely stiff and will therefore add displacement when the anterior pins are tightened.

B Requirements

Requirements	Type of requirement	Number
Pins		
• The individual pin tip force may not exceed the maximum force that is currently clinically used. Currently a pin is tightened to a torque of 0.45 Nm, this results in approximately 450 N [34]	Demand	1
• Each inserted pin may not deform plastically under the maximum force on this pin ¹	Demand	2
• During the traction period of 3 months the pins may not totally penetrate the skull	Demand	3
• Each inserted pin may not deform plastically during a maximum traction force of 600 N ²	Demand	4
• The pins may not be made out of a ferro-magnetic material	Demand	5
• The pins may not move with respect to the halo	Demand	6
• Pin forces may not be determined measuring torque	Wish	7
• Pin tips should not unintentionally transfer heat due to radiofrequency of MRI to the cranium	Wish	8
• The currently used pins are to be used in the new halo	Wish	9
• The length of the part of the pins sticking out of the halo should be as small as possible ³	Wish	10
• The number of pins should be as small as possible	Wish	11
• Conventional anterior pin placement should be changed for cosmetic reasons	Wish	12
Halo		
• The halo must provide an interface for the pins to be attached to the cranium of a patient	Demand	13
• The halo may not plastically deform at a maximum traction force of 600 N	Demand	14
• The halo must have an overall distance between 15 and 20 mm to the cranium of the patient to allow for proper cleaning[35]	Demand	15
• The halo must ensure that each pin remains the minimum required pin force of 200 N	Demand	16
• The halo allows a nodding movement of the head of the patient	Demand	17
• The halo may not break at a traction force of 600 N (safety margin of 2)	Demand	18
• The halo may not break at pin forces up to 600 N	Demand	19
• The halo may not be made out of a ferro-magnetic material	Demand	20
• The halo should provide a mechanism so that the pins are never able to penetrate the skull	Demand	21
• The halo should not cover the posterior cranium	Wish	22
• The halo should consist of the least amount of material	Wish	23
• The weight of the halo may not exceed 2 kg for the ease of handling during placement	Wish	24
• The production method of the halo is an additive manufacturing one	Wish	25
• The halo should cover the least area of a patient's cranium to allow for cleaning and scratching purposes	Wish	26
• The halo should not have a bulky look. Bulky is herein defined as a subjective measure and based on opinions	Wish	27
Connection of traction force to halo		
• The halo must provide an interface for the traction force to be applied to	Demand	28
• The axis of degree of freedom for the patient should be the nodding movement of the head	Demand	29
• The axis of rotation is positioned slightly anterior to the connection of C1 vertebrae to the skull	Wish	30

Table 6: A summary of the criteria for a newly designed halo. Some criteria are demands which should at least be met by the design. The other criteria are wishes by either the designer, patient or clinician and are desirable but not necessary.

¹This value was derived from the literature and should mimic the force generated by applying a torque of 0.45 Nm. Approximately 450 N was been found to be the maximum at a torque of 0.45 Nm.

²Safety margin of 2, assuming that 300 N is the maximum amount of traction force, taking into account dynamic effects e.g., when walking.

³During daily life activities (such as getting dressed) the patients should be bothered as little as possible by the length of pins.

C Design concepts









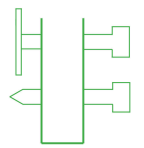
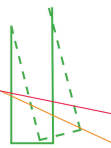
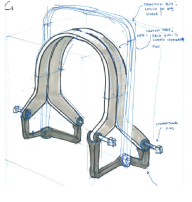
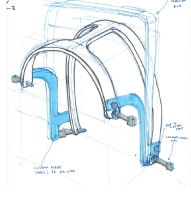
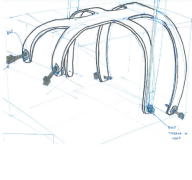
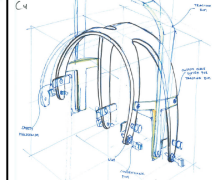
Ring shape	Headphones 	Double "C-shaped" connected 		
Pin position	Current positions 	Kevin's positions 		
Locking of the pin	Locking with a counter nut 	Alternative locking mechanisms 		
Traction rim solution	Integrated in the halo 	Not integrated within the halo 		
Safety mechanism (mechanical solutions)	Additional pin 	Optimize displacement 		
CONCEPTS				

Figure 39: Subproblems associated with the design of a new halo. Combinations of these subproblems are summarized in design concepts. 4 design concepts are presented here.

Subjective analysis on the 4 design concepts was performed, by discussing these with the clinicians at UMC Utrecht. Decision was made on the last design concept. This design concept is illustrated in Figure 40, where the yellow part is the attachment for the traction rim.

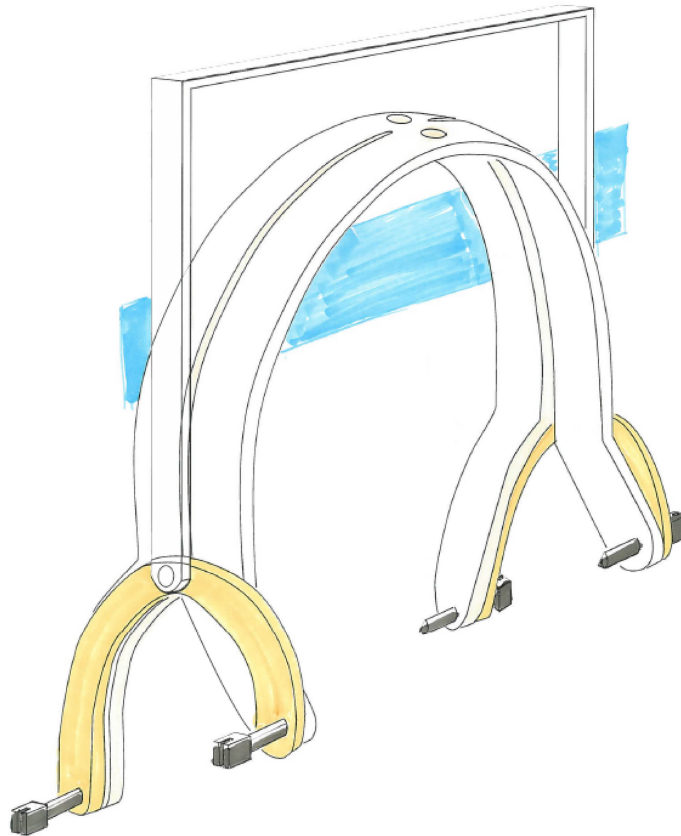


Figure 40: Design drawing of chosen concept. The yellow part is where the traction rim will be attached to.

D Novel Halo - Parameter Determination

D.1 Geometry determination

The skull of the cadaver head was scanned using Computed Tomography. Global shape geometry of the skull determined the contour of the C-shapes and the curvature of both ends of the C-shapes, as shown in Figure 41 were obtained.

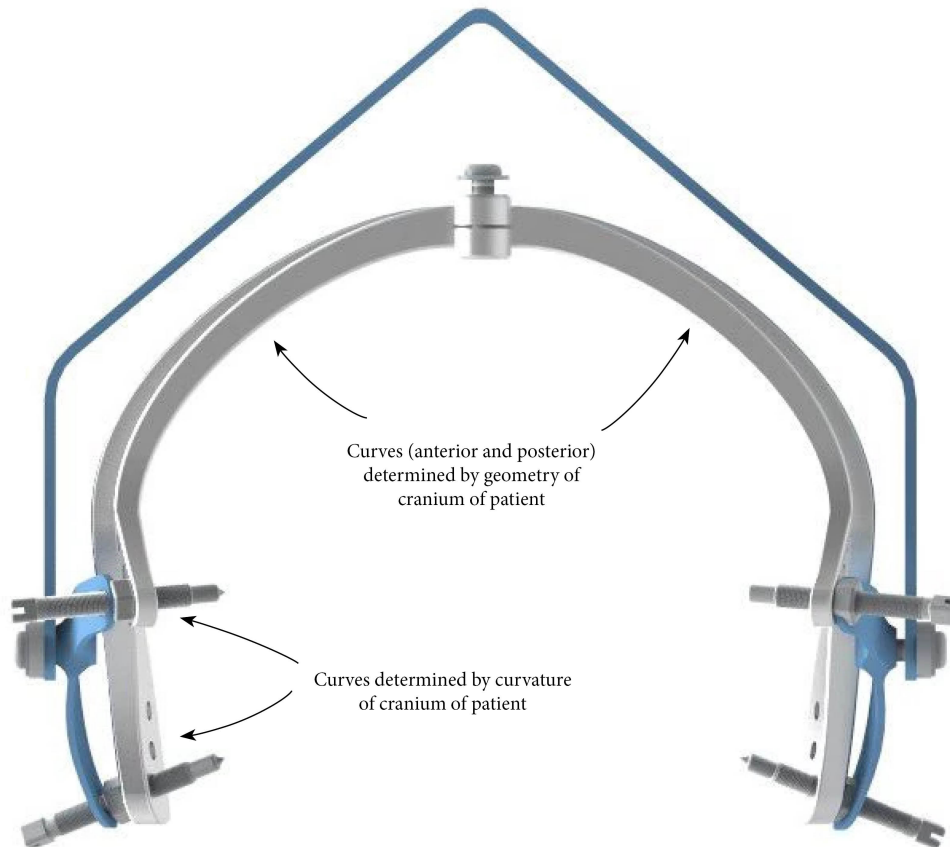


Figure 41: Global curvatures of the halo were determined from the geometry of the skull and skin of the cadaver. A minimum distance of 15-20 mm was kept between the halo and epidermis of the patient to allow for proper cleaning.

The remaining dimensions of both C-contours, such as the thickness and width, as illustrated in Figure 42, were determined by the maximum allowable displacement at each C-contour. By applying this condition to the model, an optimization criteria in Solid Edge ST 10 iteratively created the estimates of these parameters. The maximum displacement at a given load would be given as input values to calculate the combinations of the thickness and depth.



Figure 42: Thickness and depth of the posterior C-contour. The thickness and depth were not constant over the entire circumference of the C-contour. The variances between 't' and 'd' over the C-contour are partially determined by an optimization algorithm in Solid Edge ST10. The ratio between the variances were imposed by the designer. E.g. 't' inferiorly should always be smaller than 't' superiorly.

D.2 Displacements at anterior and posterior pin sites - FEM

FEM analysis of both the anterior C-contour and posterior C-contour was conducted. The results of this analysis are presented in Figure 43. The dimensions of both C-contours are the result of the imposed displacement at the pin sites in combination with the material properties of the novel halo. Both C-contours are able to displace 5 mm at a force of 450 N. A maximum force of 600 N was applied at one pin site before failure. According to this FEM analysis, no alarming stresses arose in the material under this maximum force.

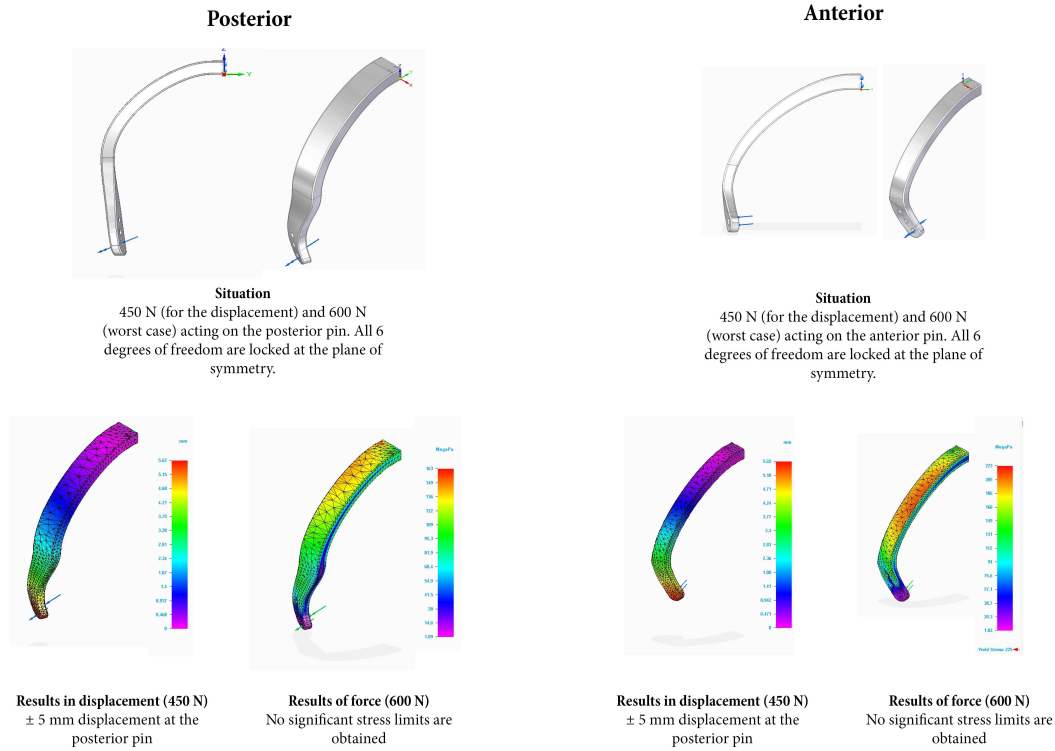


Figure 43: Displacements and forces on the posterior and anterior C-contour

D.3 Displacement at anterior and posterior pin sites - experimental measurements

Measuring the stiffness of the C-contours of the novel halo at posterior and anterior pin sites was realized by attaching a force gauge with a maximum capacity of 1000 N. The setup is shown in Figure 44. A digital dial indicator with an accuracy of 0.01 mm was used to measure the displacement. Starting at a load of 30 N with increments of 30 N, the displacements were measured. The forces were translated to the directions of the pins, by dividing the force-values to the cosine of 0.4 and 0.61 radians for the anterior and posterior C-contours respectively. The results are illustrated in Figure 45. In these graphs, the bandwidth of Young's moduli of the material as given by Oceanz, is included.



Figure 44: Overview of the test setup for measuring the stiffness at both the posterior and anterior pin sites.

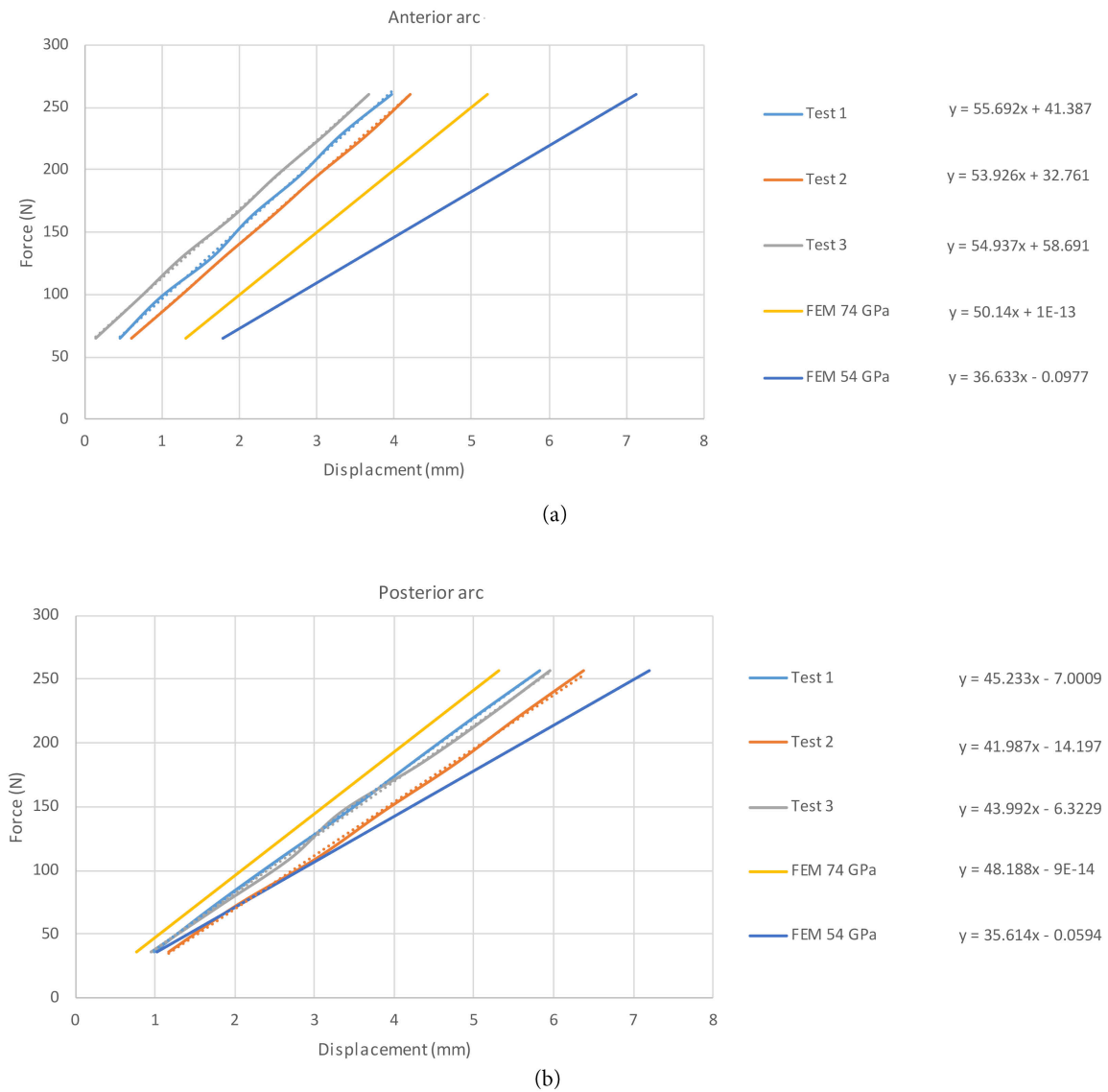


Figure 45: Results obtained from 3 tests to determine the displacements of the anterior and posterior C-contour the novel halo. The slope of the line was the measured stiffness, which was roughly $55 \frac{N}{mm}$ for (a) and $44 \frac{N}{mm}$ for (b). According to FEM the theoretical difference in stiffness should be between $50 \frac{N}{mm}$ and $36 \frac{N}{mm}$ for the anterior C-contour and between $48 \frac{N}{mm}$ and $35 \frac{N}{mm}$ for the posterior C-contour. This was found by applying the maximum (74 GPa) and minimum (54 GPa) Young's modulus values, which were provided by Oceanz (see Figure 35), to the CAD model

E Relationship between Torque and Force in the Bremer halo

A torque wrench was used to measure the amount of torque to tighten the pins. Manually 0.45 Nm was applied to the pins and the force was estimated. The setup is illustrated in Figure 46. The results of 5 consecutive tests are presented in Table 7. The variations are attributed to human error during the application of torque to the pin.

Trial	Force (N)
Mean $\pm \sigma$	369 \pm 24
1	370
2	395
3	340
4	396
5	344

Table 7: Force measurements when a torque of 0.45 Nm was applied. The average of the 5 tests is 369N.

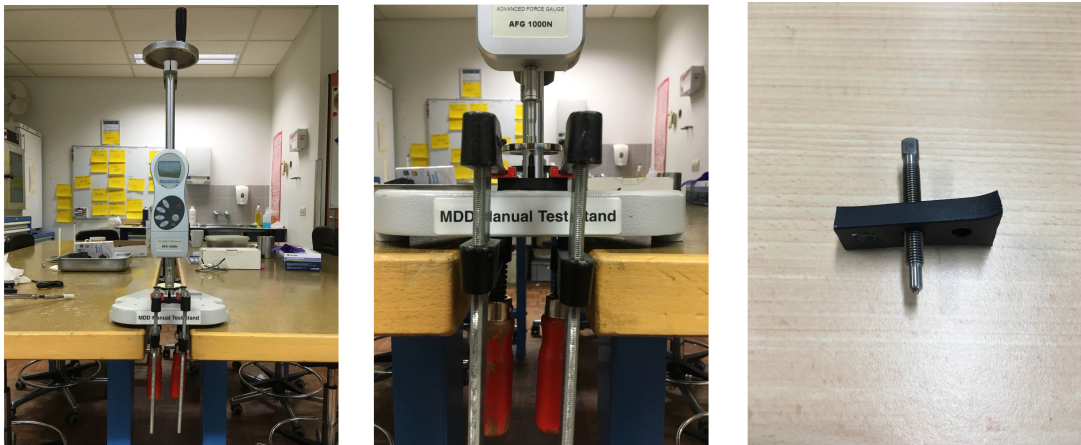


Figure 46: Overview of the test setup for determining the relationship between torque and force in the Bremer halo. Note that during such tests all conditions remained unchanged and would thus result in quite consistent values. During pin tightening in a clinical setting, the conditions may not be the same.

F Strain Gauges

F.1 Anterior ring of novel halo

Figure 47 illustrates the spots where the strain gauges should be placed on the anterior C-contour. The stresses corresponded to a force of 600 N at the pin site location. This was the maximum load the ring was expected to be able to bear. The corresponding stresses in the C-contours were tensile stresses at a level well below the yield stress of the material and therefore, no plastic deformation would occur. Strain gauges should be placed at the spots where stresses and so also strains are relatively high as seen in Figure 47.

To make a complete Wheatstone bridge, at each strain gauge spot, two strain gauges are needed (namely, each gauge already contains two strain gauges, so actually four gauges were used per spot). A Wheatstone bridge is a configuration of connecting strain gauges and/or resistances to calculate a voltage difference or an unknown resistance. One gauge was placed on the inferior side (side of the cranium) and the other gauge on the superior side of the halo.

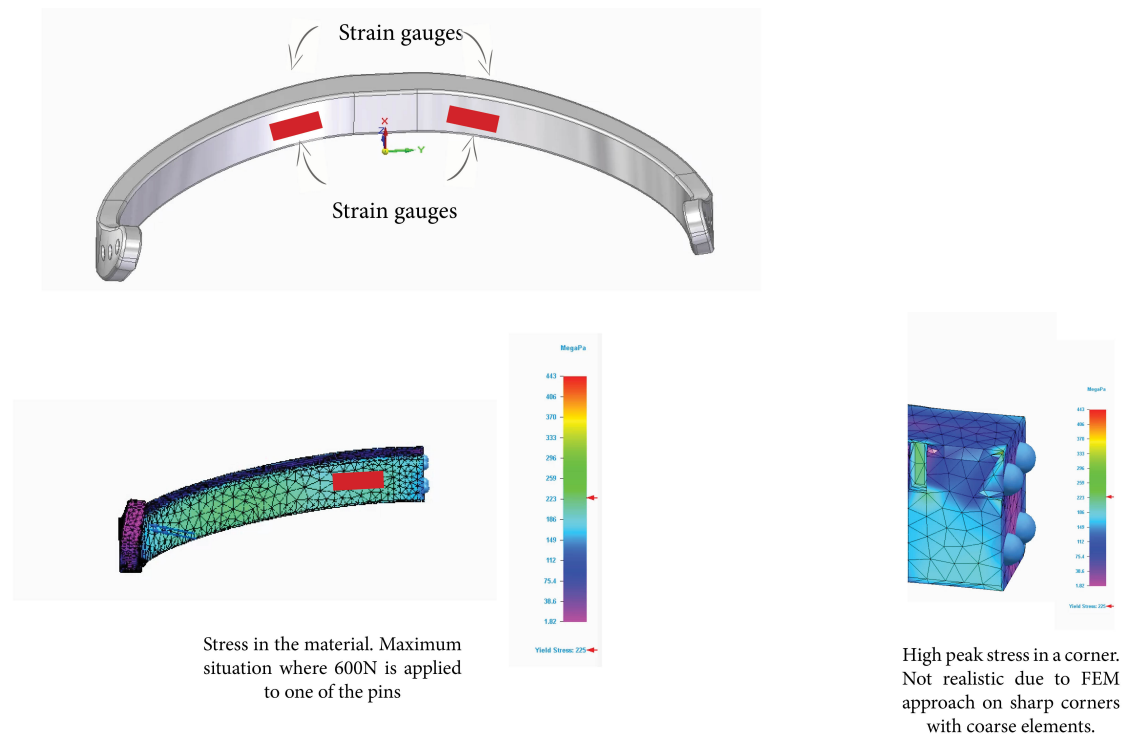


Figure 47: Overview of the spots where the strain gauges were placed in the anterior C-contour on the new halo.

F.2 Posterior ring of the novel halo

Figure 48 illustrates the spots where strain gauges were placed on the posterior C-contour. The stresses seen in Figure 48 corresponded to a force of 600 N on one of the pins. This force created tensile stresses at the cranium part of the ring. This is the spot the strain gauges should be placed. The reason for using 4 strain gauge spots instead of 2 spots, is that with 4 spots the effect of the bridge connector (part of halo, but not the Wheatstone bridge) could be measured.

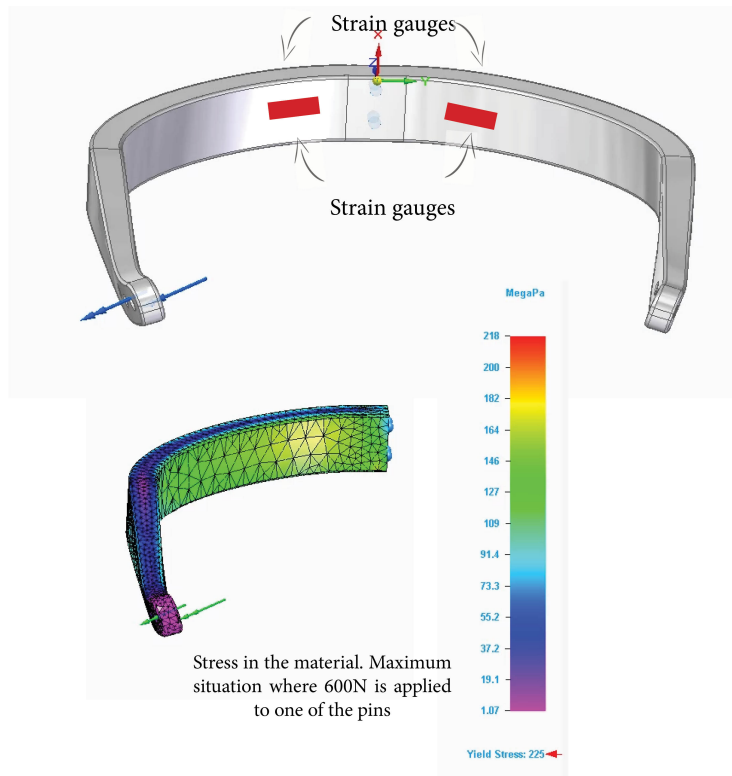


Figure 48: Overview of the spots where the strain gauges were placed in the posterior ring of the new halo.

F.3 Calibration of strain gauges

Calibrating strain gauges was done by adding calibrated weights to the posterior and anterior C-contour, as illustrated in Figure 49. The voltage output was measured at a given weight. The relationship between the force and voltage became known. The calibration graphs for all four pins are shown in Figure 50.

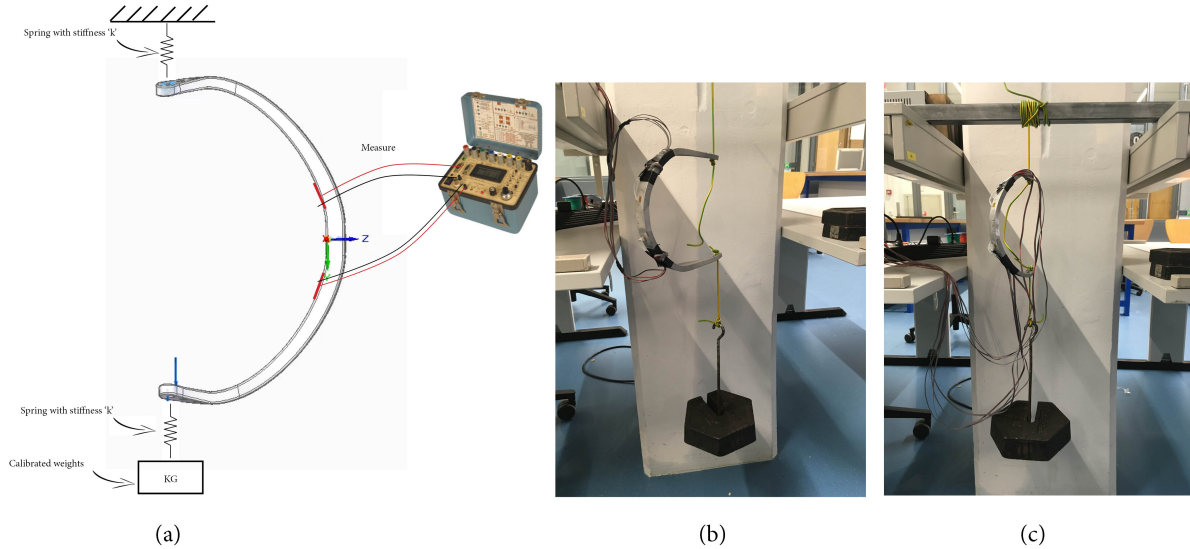


Figure 49: (a) Schematic setup for the calibration of the C-contours of the novel halo. (b) Calibration setup for the posterior C-contour. (c) Calibration setup for the anterior C-contour. Consecutive weights were added, starting at 0 kg and ending up at 10 kg.

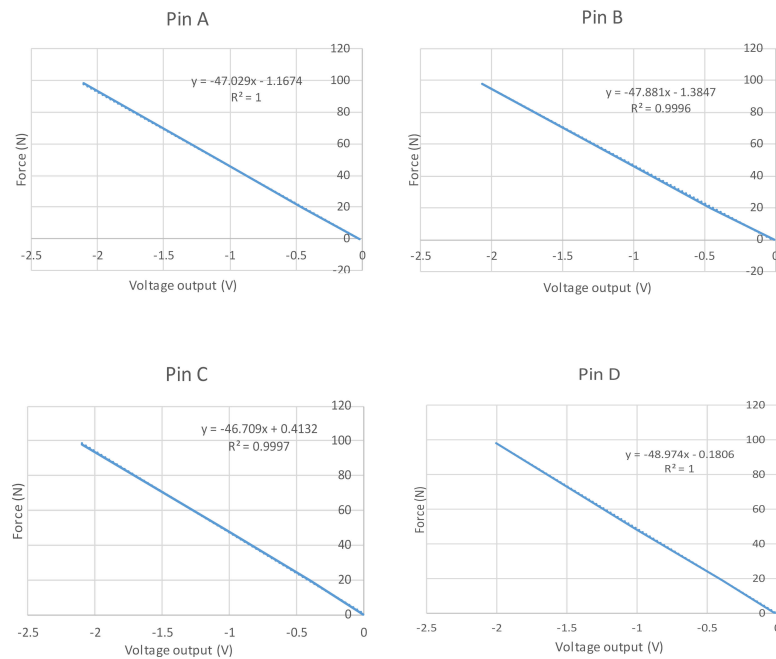


Figure 50: Calibration graphs of each of the pins. The formula's of these graphs were used to convert the strain gauge data to a force acting on a pin.

F.4 Technical data of strain gauges

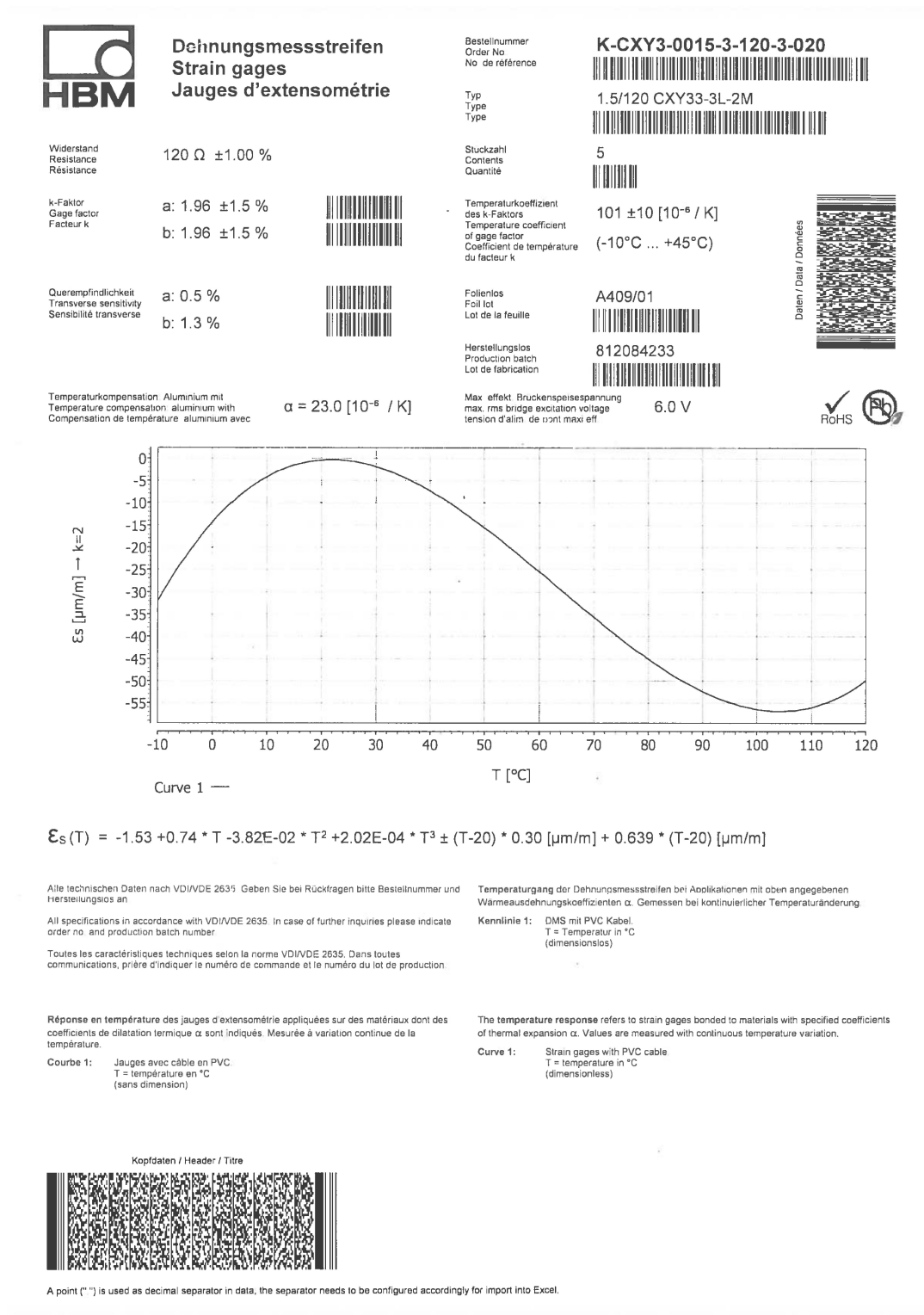


Figure 51: Technical data sheet of the strain gauges acquired from HBM.

G Traction Force

Usually 20 kg, or 50% of the body weight of a child, is used as a maximum force during the HGT treatment[4][6][41][42]. In this study a maximum weight of 30 kg was considered, since that would cover 95% of the population of Dutch children. This information was obtained from <https://dined.io.tudelft.nl/en/database/tool>, which is an anthropometric database mainly for the Dutch population. The connection of the novel halo did not fail during 36 kg of traction.

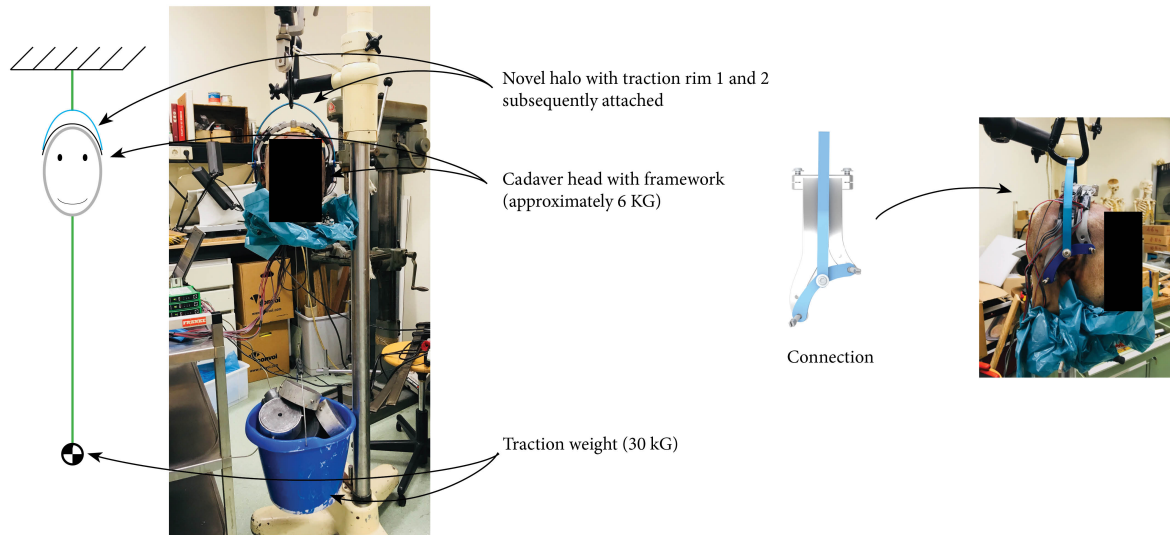


Figure 52: The novel halo applied to the cadaver head. In total 36 KG (30 KG weight, 6 KG head) was hung to the connection. No issues were recorded.

Thanks for reading
Wolf Botterman